ISSN 2162-5298 (Print)
ISSN 2162-5301 (Online)
DOI:10.17265/2162-5298

David Publishing Company
www.davidpublisher.com

Journal of Environmental Science and Engineering A

Volume 7, Number 3, March 2018

From Knowledge to Wisdom

Journal of Environmental Science and Engineering A

Volume 7, Number 3, March 2018 (Serial Number 69)

David Publishing Company
www.davidpublisher.com

Publication Information:
Journal of Environmental Science and Engineering A (formerly parts of Journal of Environmental Science and Engineering ISSN 1934-8932, USA) is published monthly in hard copy (ISSN 2162-5298) and online (ISSN 2162-5301) by David Publishing Company located at 616 Corporate Way, Suite 2-4876, Valley Cottage, NY 10989, USA.

Aims and Scope:
Journal of Environmental Science and Engineering A, a monthly professional academic journal, covers all sorts of researches on environmental management and assessment, environmental monitoring, atmospheric environment, aquatic environment and municipal solid waste, etc..

Manuscripts and correspondence are invited for publication. You can submit your papers via Web Submission, or E-mail to environmental@davidpublishing.org, environmental@davidpublishing.com or info@davidpublishing.com. Submission guidelines and Web Submission system are available at http://www.davidpublisher.com.

Editorial Office:
616 Corporate Way, Suite 2-4876, Valley Cottage, NY 10989, USA
Tel: 1-323-984-7526, 323-410-1082
Fax: 1-323-984-7374, 323-908-0457
E-mail: environmental@davidpublishing.org; environmental@davidpublishing.com; info@davidpublishing.com

Abstracted/Indexed in:
Googel Scholar
CAS (Chemical Abstracts Service)
Database of EBSCO, Massachusetts, USA
Chinese Database of CEPS, Airiti Inc. & OCLC
Cambridge Science Abstracts (CSA)
Ulrich's Periodicals Directory
Chinese Scientific Journals Database, VIP Corporation, Chongqing, China
Summon Serials Solutions
ProQuest

Subscription Information:
Price (per year):
Print $600, Online $480
Print and Online $800

David Publishing Company
616 Corporate Way, Suite 2-4876, Valley Cottage, NY 10989, USA
Tel: 1-323-984-7526, 323-410-1082; Fax: 1-323-984-7374, 323-908-0457
E-mail: order@davidpublishing.com
Digital Cooperative Company: www.bookan.com.cn

David Publishing Company
www.davidpublisher.com

Journal of Environmental Science and Engineering A

Volume 7, Number 3, March 2018 (Serial Number 69)

Contents

Journal of Environmental Science and Engineering A 7 (2018) 101-107
doi:10.17265/2162-5298/2018.03.001

Application of Hydrological Model to Simulate Rainfall-Runoff into An Khe Reservoir in the Ba River Basin, Vietnam

Nguyen Van Hieu[1, 2], Can Thu Van[3] and Vu Minh Cat[2]

1. Ministry of Natural Resources and Environment, Ha Noi 100000, Vietnam

2. Thuyloi Universiry, Ha Noi 100000, Vietnam

3. Hochiminh City University of Natural Resources and Environment, HCM City 700000, Vietnam

Abstract: The BR (Ba River) basin is one of 9 main river basins in Vietnam. In the past 20 years, natural hazards such as flood and inundation have been complex and increased dramatically in both frequency and intensity in the BR basin. Recently, there have been approximately 198 large and small operating reservoirs which lead to increase natural hazards in the river basin. An Khe reservoir, one of big reservoirs in the upstream of the Ba river, impacts significantly on flooding in the downstream. This paper uses hydrological model to simulate the flows as a basic for the safety operation of An Khe reservoir in order to prevent the downstream floods. The results indicate the Nash-Sutcliffe coefficient higher than 0.8 is stable and reliable parameter.

Key words: Ba river basin, flood, An Khe reservoir, hydrographic model, rainfall-runoff.

1. Introduction

1.1 Natural Condition of the Ba River Basin

The BR (Ba River) basin belongs to the administrative boundaries of 20 districts and one city of the three provinces in Central Highlands including Kon Tum, Gia Lai, Daklak and the Southern Central coastal province of Phu Yen.

The BR basin is mostly L-shaped with narrow upstream and downstream and middle river basin in an average of 48.6 km wide and the widest of 85 km. BR flows into the sea in three main directions: (1) Northwest-Southeast direction is from Ngoc Ro mountain peak of about 1,549 m high of Truong Son range to An Khe; (2) North-South direction is from An Khe to Hinh river and (3) West-East direction is from Hinh river into the East Sea at Tuy Hoa city.

The BR basin has an area of 14,140 km^2, the river length is approximately 388 km and the river density is about 0.22 km/km^2. The river basin expands less than others.

The river has many tributaries including more than 50 tributaries with the length of over 20 km and 19 tributaries with a basin area of over 100 km^2. There are three main tributaries: Ayun, Krông Hnang and Hinh river.

The Ayun river, is the largest tributary of the Ba river, originates from the Cong Lak mountain peak with a height of 1,720 m in the North-South direction and then turns to the Northeastern direction to the confluence with the BR at Cheo Reo. The main river length is 291.8 km and the basin area is 2,874 km^2.

Krông Hnang river, is the second largest tributary of the Ba river, originates from the Chu Tun Mountain peak with the height of 1,215 m in Northeast-Southwest direction and then flows in the North-South direction and moves to the arc-shaped in the opposite direction to the confluence with the BR at the boundaries of Gia Lai and Phu Yen provinces. The

Corresponding author: Nguyen Van Hieu, Ph.D. student, research fields: hydrology and water resources.

length of Krông Hnang river is 130 km and the basin area is 1,761 km^2.

The Hinh river, is the third largest tributary of the BR, originates from Chu Hreu Mountain peak with the height of 2,051 m in Southwest-Northeast direction and then flows in many directions, finally followed by South West-North East to the confluence with BR at Son Hoa. The Hinh river has a basin area of 1,040 km^2 and a length of about 59 km (Fig. 1) [1, 2].

1.2 Characteristics of An Khe Flows

In the BR basin, the fluctuations of seasonal flow are quite complex. Floods in this river happen two to three months sooner or later than that in other rivers. The length of annual flood season varies in years: 2 to 3 months or 5 to 6 months. Because the Southwest monsoon comes strongly from the beginning of rainy seasons (May), flood seasons in the basin start early. In the case that typhoons and tropical depressions from the East Sea appear at the end of rainy season, the flood season will last, even to next January. Particularly, the Hinh river and other small streams in the downstream are impacted solely by the climate of the East Truong Son, so the seasonal flow is more stable.

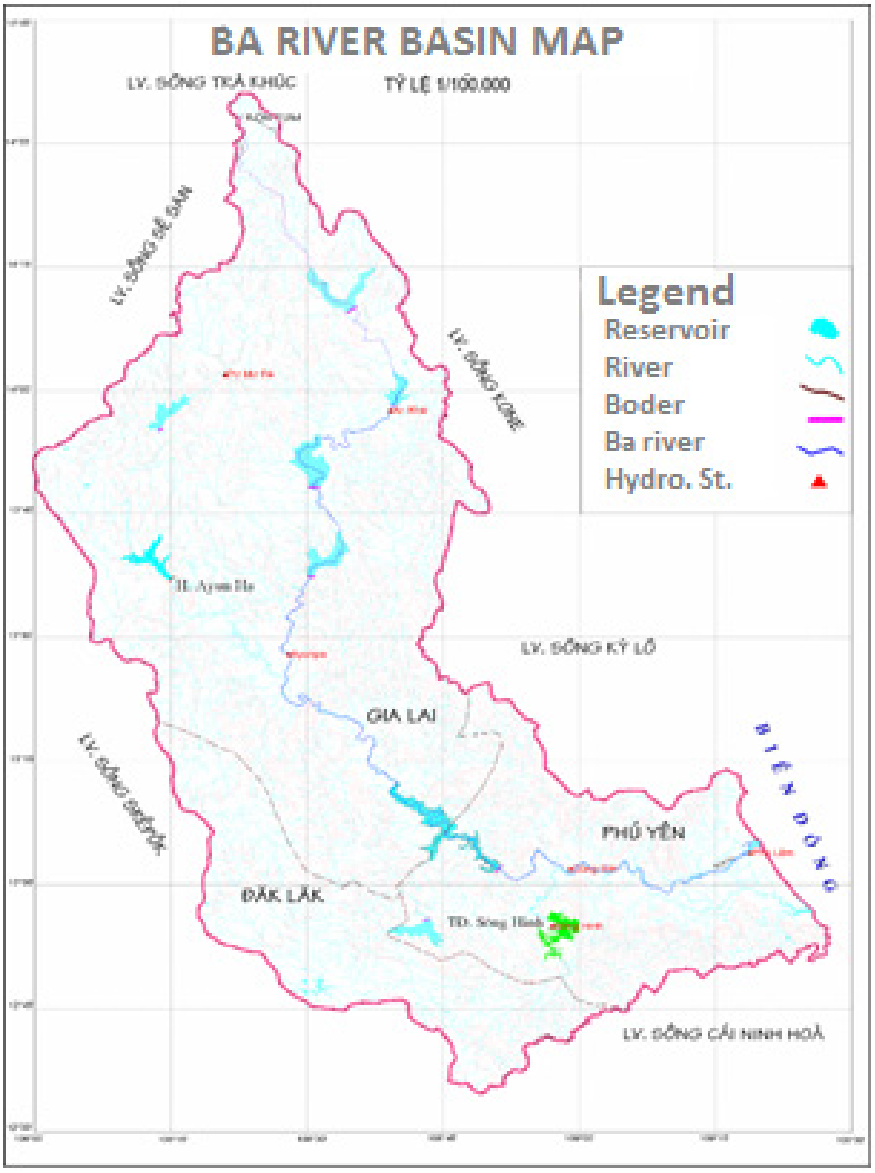

Fig. 1 Ba river system map.

In the upstream of the BR: Flood season lasts 3 to 4 months from September to December. The annual flood flow rate was high (the highest was up to 90% in 1983 and 1998, the lowest was 30% in 1982). The highest flow was in October, occupying average 46% of flood season flow [1].

In the An Khe tributary, flood water level was higher than WWL (Water Warning Level) II in 21 years, which appeared 2 times in 2 months of 7 years and higher than WWL III in 15 years, which appeared 2 times in 2 months of 4 years. The typical floods were in years: about 1.05 m higher than WWL III in 1980; around 1.98 m higher than WWL III in 1981 and approximately 1.65 m higher than WWL III in 2007. These years including 1978, 1979, 1982, 1989, 2006 and 2012 have small floods [1, 3].

The An Khe-Ka Nak reservoirs located in the upstream of the BR were built together to improve the efficiency of electricity generation. Ka Nak reservoir regulates about 285.5 million m^3/yr and provides a water level of 357 m for electricity generation at An Khe hydropower plant.

According to design for flow rate from Ka Nak reservoir to hydropower plant, the average flow rate is 11 m^3/s, the largest flow is 42 m^3/s. With An Khe reservoir, the average and highest flows rate are 9.6 m^3/s, and 50 m^3/s respectively [1, 4].

According to reservoir operation data in 2 years 2011 and 2012, in the dry season, the flow rate of Ka Nak reservoir was the highest of about 30 m^3/s, average of 15 m^3/s and the smallest of about 13.1 m^3/s. Meanwhile, An Khe reservoir had the highest flow rate of about 48-50 m^3/s and average 24 m^3/s. By the end of the dry season in 2012, the water level of Ka Nak reservoir was quite high to supply a large amount of water for the operation of An Khe factory. In the flood season year 2012, the flow of An Khe reservoir was very small without floods while Ka Nak reservoir decreased electricity generation to accumulate water, but still 7.0 m lower than that in statistics (Fig. 2) [1].

The inundation region in downstream of the An Khe reservoir: An Khe town, located on the National Road 19 from Binh Dinh town (An Nhon) to Pleiku, is between An Khe Pass (border Tay Son district, Binh Dinh province) and Mang Yang Pass (border Mang Yang district, Gia Lai province). According to An Khe Hydrological Station data, many areas become inundated due to the increase in flood water level, including the downstream areas which are about 8.5 km far from An Khe reservoir and approximately 33 km far from Kanak reservoir. Therefore, flood prevention depends on the operation of these reservoirs. The relationship between total utilizable storage capacity of An Khe and Ka Nak reservoirs and the highest total flow volume in 10 days within the period of 32 years revealed that the total flood volume was higher than utilizable storage capacity in 12 years, in which, the total flood volume is 0.6 times higher than utilizable storage capacity in 11 years. Therefore, in devastating flood years, both two lakes discharge to death water level to control floods but it is not able to control floods thoroughly. As a result, reservoirs will only be able to support flood reductions for downstream area when they were assigned additional missions [1, 5].

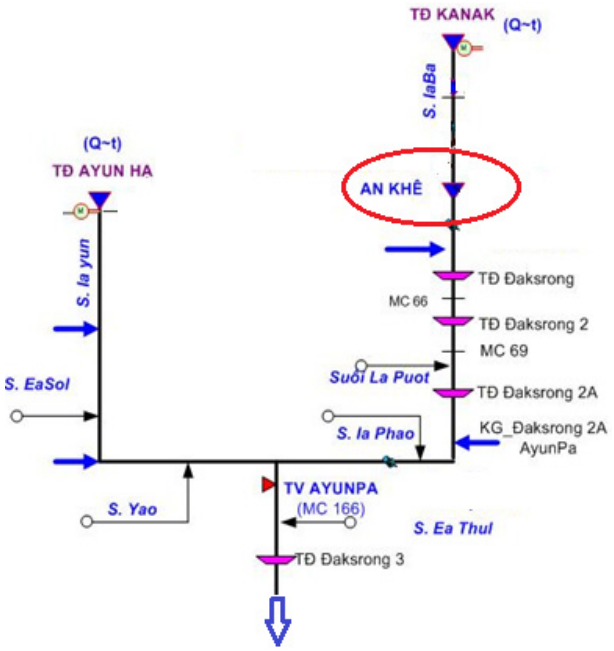

Fig. 2 An Khe reservoir location diagram.

2. Methodology

2.1 Hydrological Models

Hydrological models can be used to determine the boundary condition for hydraulic models. In hydrology, there are many functions of water concentration and there are many methods to build it. The isochronous flow method is based on the variability of flow rate to determine the area of isochronous flow and the concentration curve of water. The unit flow line method was first proposed by Sherman, and was developed and completed by many authors. The Kalinin-Miliukov concentration curve and the Nash unit hydrograph are shown as the adjustment in the rivers or in the river basins equivalent to the adjustment of a linear reservoir system.

Based on this assumption, although the step and specific solution of methods are different, but both of them lead to the concentration curve of water having a similar form as the Gamma function. Some of the synthetic unit flowlines such as Snyder, SCS and Clark... were developed to calculate for the river basins without data of flow measurement [6-8].

2.2 Structures of NAM Model (Rainfall-Runoff Model)

The NAM model stands the acronym in Danish "Nedbør Affstrømnings Model", meaning rainfall-runoff model. NAM is a deterministic, conceptual and lumped hydrological model, was built in 1982 at the Faculty of Hydrology, DHI (Danish Hydraulic Institute), University of Technology Denmark. The NAM model is based on the principle of five storages: snow storage; surface storage; lower zone storage; upper groundwater storage and underground water storage.

The basic inputs for the NAM model include: model parameters, initial conditions, meteorological data, flow data for model calibration and verification [2, 6, 9].

The NAM model is based on the structures and physical equations which are used together with the semi-experience formula. This is a lumped model which treats a whole catchment as a single unit. As a consequence, basin characteristics are represented as average values for the hydrologic processes over the catchment as a whole.

The model structure is shown in Fig. 3. The NAM model simulates the rainfall-runoff process by continuously calculating the amount of water in storages that are related to each other, which depicts the physical composition of the different basins. These storages include surface storage, lower zone storage and underground storage. Furthermore, the NAM model allows the processing of human intervention in the hydrological cycle, such as irrigation and groundwater extraction [9, 10].

Based on meteorological data, the NAM model generates flow as well as information about soil layers in the hydrological cycle, such as the temporal variability of evapotranspiration, soil moisture, intake of underground water, underground water level, etc..

The conceptual flow of the basin is divided into surface flow, sub-surface flow and underground flow.

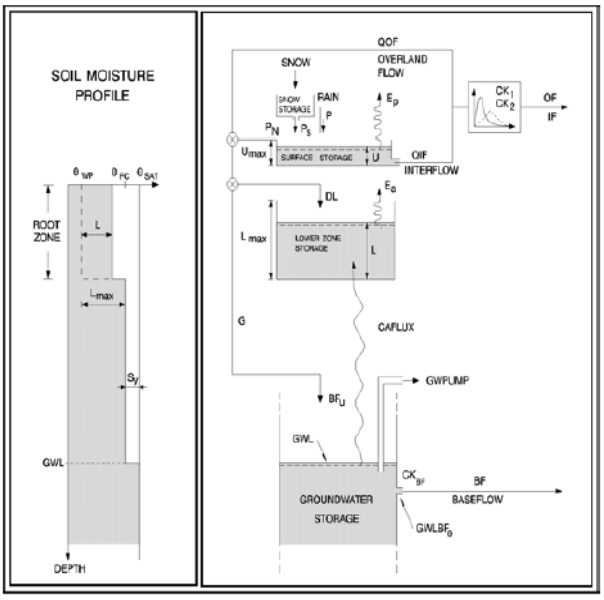

Fig. 3 Structure of NAM model for rainfall-runoff simulation.

2.3 Composition of Rainfall-Runoff Model (NAM)

Maximum water content in surface storage (U_{max}): represents the cumulative total water content of interception storage and storage in the upper layers of soil.

Maximum water content in root zone storage (L*max*): represents the maximum moisture content in soil in the root zone.

Snow storage: rainfall will be held in the snow storage when temperature is below 0 °C, if temperature is higher than 0 °C, it will move to the surface storage:

$$Q_{melt} = \begin{cases} CSNOW\ TEMP\ khi\ TEMP > 0 \\ 0 \qquad\qquad khi\ TEMP\ \delta\ 0 \end{cases}$$

CSNOW = 2 mm/day/K—snowmelt coefficient during the day.

Evaporation: If the amount of moisture U in the surface storage is less than this demand, it will get moisture from the root layer followed by the rate E_a. E_a is proportional to potential evapotranspiration E_p:

$$E_a = E_p\ L / L_{max}$$

Surface runoff: When the surface storage overflows, $U \geq U_{max}$, the amount of water that exceeds the P_N will form the surface runoff and infiltrate. QOF is part of P_N, participates in surface runoff formation, it is proportional to P_N and changes linearly with relative humidity, L/L_{max}, of root layer:

$$QOF = \begin{cases} CQOF \dfrac{L/L_{max} - TOF}{1 - TOF} P_N\ khi\ L/L_{max} > TOF \\ 0 \qquad\qquad khi\ L/L_{max} \leq TOF \end{cases}$$

CQOF is coefficient of overland flow ($0 \leq CQOF \leq 1$).

TOF is threshold value of overland flow ($0 \leq TOF \leq 1$).

Interflow: Interflow QIF, is assumed to be proportional to U and linearly transformed with the relative humidity of the root tank:

$$QIF = \begin{cases} (CKIF)^{\square 1} \dfrac{L/L_{max} \square TIF}{1 \square TIF} U\ khi\ L/L_{max} > TIF \\ 0 \qquad\qquad khi\ L/L_{max}\ \delta\ TIF \end{cases}$$

CKIF is time constant for routing interflow; TIF is root zone threshold value for interflow ($0 \leq TIF \leq 1$) [9].

3. Results

Simulation result from 1st January 1986 to 31st December 1986 is shown as Fig. 4.

Simulation result from 1st January 1988 to 31st December 1988 is shown as Fig. 5.

Simulation result from 1st January 2003 to 31st December 2003 is shown as Fig. 6.

Results of error evaluation are in Table 1.

Hydrograph error:

$$NASH(EI) = 1 - \frac{\sum (Qcal - Qobs)^2}{\sum (Qobs - Qobsave)^2}$$

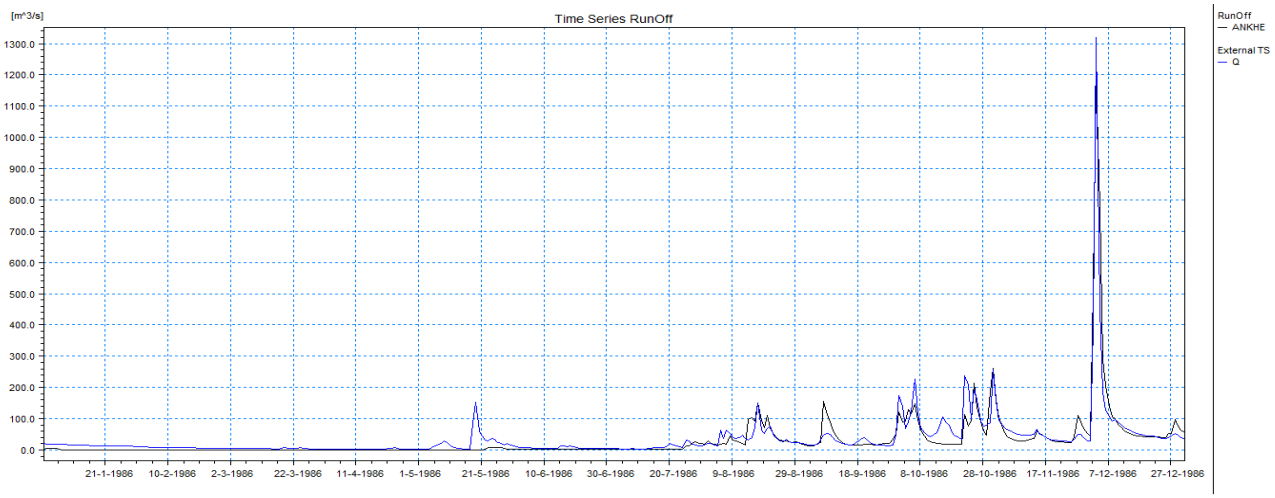

Fig. 4 Comparing observed and simulated flow rate to the An Khe reservoir in 1986.

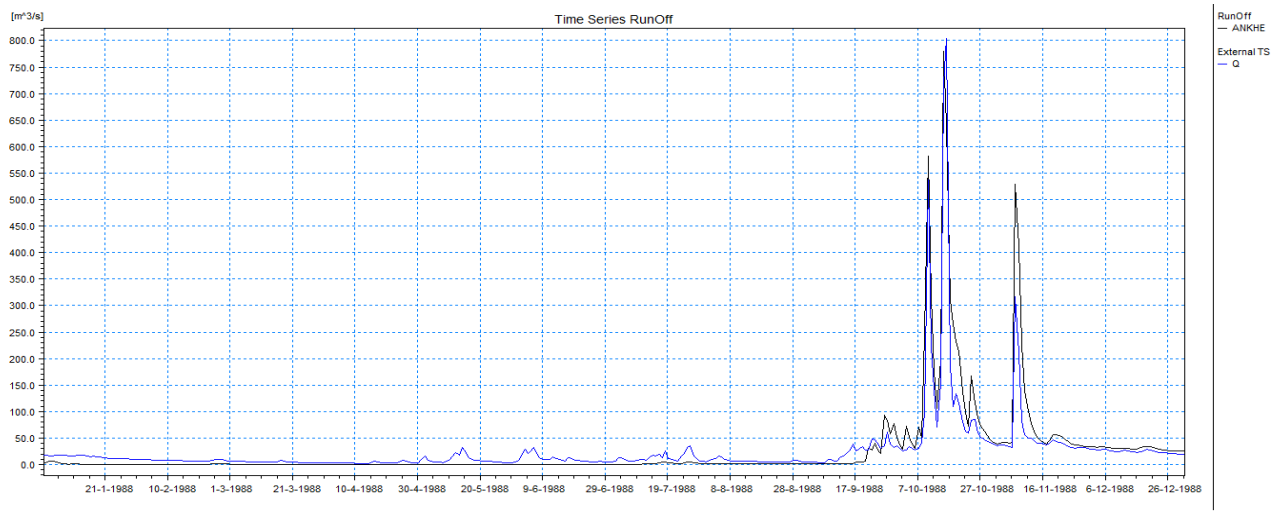

Fig. 5 Comparing observed and simulated flow rate to the An Khe reservoir in 1988.

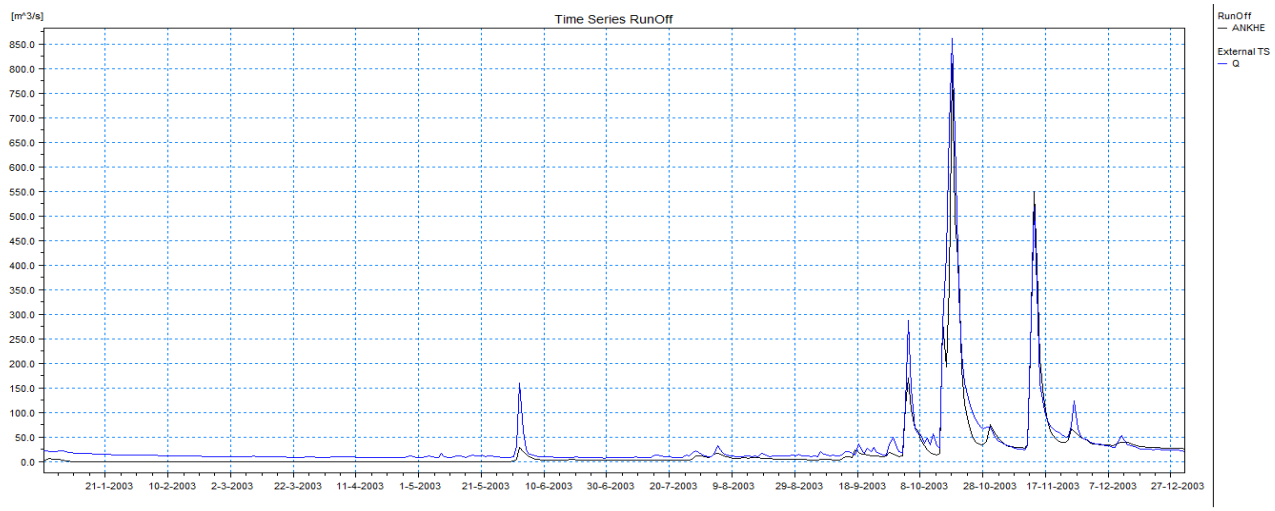

Fig. 6 Comparing observed and simulated flow rate to the An Khe reservoir in 2003.

Table 1 Results of error evaluation.

Indicators	1986	1988	2003
Nash	0.86	0.82	0.89
ΔQmax (%)	9.8	2.9	6.1

Table 2 Results of NAM model parameters.

No.	Parameters	Value
1	Umax	15.3
2	Lmax	120
3	CQOF	0.61
4	CKIF	304.2
5	CK12	21.5
6	TOF	0.507
7	TIF	0.328
8	TG	0.134
9	CKBF	2507

in which, Qcal—calculated flood flow rate (m^3/s);

Qobs—observed flood flow rate (m^3/s);

Qobsaver—average observed flood flow rate (m^3/s).

Flood peak error ($\Delta Qmax$):

$$\Delta Qmax = \left| \frac{Q_{max}^{tt} - Q_{max}^{td}}{Q_{max}^{td}} \right|$$

in which: Q_{max}^{tt}—simulated flood peak;

Q_{max}^{td}—observed flood peak.

Model parameters: results of NAM model parameters are in Table 2.

4. Conclusions

Based on three flood events in the past with different characteristics, the study chose 3 years having typical floods which included:

The flood in 1986: flood peak is about 1,320 (m^3/s);

The flood in 1988: flood peak is about 804 (m^3/s);

The flood in 2003: flood peak is about 862 (m^3/s).

With different flood levels, the model parameters still give results quite good: the Nash-Sutcliffe coefficient is higher than 0.8 as good simulation level and flood peak errors are always smaller than 10% as acceptable error level. Therefore, NAM model could be used to simulate rainfall-runoff into An Khe reservoir for flood prevention and control in the downstream of the Ba river.

References

[1] Luong, H. D. 2016. "Research Methodology of Operation Reseroirs System to Flood Control in Ba River Basin." Ph.D. thesis, Vietnam Institute of Meteorology, Hydrology and Climate Change.

[2] Van, C. T. 2011. "Research and Application of MIKE FLOOD Model to Assess the Inundation Level of Ba River." Master thesis, Thuyloi University, Hanoi.

[3] Nguyen, H. K. 2010. "Operation Technology Construction Research of Conjunctive Reservoir System to Guarantee Flood Prevention, Flood Retarding, Safety for Reservoir Operation and to Use Sensibly Water Resources in Lowest Season on Ba Basin." Code KC.08.30/06-10. State Level Projects.

[4] Luong, H. D. 2012. "Some Characteristics of Rain and Flood in Ba River Basin in Inter-Reservoir Operation to Control Downstream Flood." *Journal of Meteorology and Hydrology* 620 (8): 32-35.

[5] Mai D. T. 2013. *Study and Develop a System for Analysis, Monitoring, Warning and Forecast of Floods, Floods and Droughts for the Ba River Basin*. Final Report of the theme of the Ministry of Natural Resources and Environment.

[6] Nguyen, H. K., and Nguyen, T. S. 2003. *Hydrographic Model*. Hanoi: Vietnam National University Publishing, p. 241.

[7] Chow, V. T., Maidment, D, R., and Mays, L. W. 1998. *Appiled Hydrology*, McGraw-Hill, ISBN 0-07-010810-2.

[8] Van, C. T., Khai, N. H., and Son N. T. 2011. "Application of Hydraulic Model to Calculate Inundation in Ba River." *VNU Journal of Science, Natural Science and Technology* 27 (1S): 273.

[9] DHI (Denmark Hydraulic Institute). 2007. "A Modelling System for River and Chanels-Mike NAM." In *User Manual Book*. Danmark: DHI Software, Water and Environment.

[10] Van C. T., and Son, N. T. 2016. "Simulation of Hydrological, Hydraulics in Mekong Delta to Assess the Impact of the Dike System to Change the Flow in Dong Thap Muoi." *Vietnam University National Scientific Journal* 32 (3S): 256-63.

Journal of Environmental Science and Engineering A 7 (2018) 108-124
doi:10.17265/2162-5298/2018.03.002

Perspectives on the Potential Migration of Fluids Associated with Hydraulic Fracturing in Southwest Florida

William C. Hutchings[1] and Richard G. Lewis[2]

1. Environmental Department, GHD Services Inc., Fort Myers 33901, USA

2. Lewis Solutions, Fort Myers 33907, USA

Abstract: The variable-density flow model—SEAWAT Version 4, was used to evaluate the hydrogeological conditions associated with hydraulic fracturing (fracking) the limestone oil reservoir in the Lower Cretaceous Sunniland Formation of Southwest Florida. This research contributes to the understanding of the controls on fluid and potential contaminant migration, following high pressure hydraulic fracturing. A hydraulic fracturing treatment used recently in this formation at the Collier-Hogan 20-3H well represents the base case simulation. Multiple stage fracturing using typical stress periods, a modelled fracture zone radius, and various injection rates were tested to evaluate the potential for horizontal and vertical fluid migration in and from the reservoir under dynamic conditions, with TDS used as a tracer. Hypothetical scenarios including preferential vertical pathways between the Sunniland Formation and the Lower Floridan aquifer Boulder Zone were also simulated. Results indicate that injected fluids do not migrate significantly in the lateral and vertical directions beyond the design fractured zone, unless a preferential pathway exists within close proximity to the fractured zone. In a worst-case scenario under the simulated conditions, vertical heads are approximately 580 meters greater than static conditions and fluids associated with hydraulic fracturing vertically migrate approximately 500 meters; therefore, the quality of the deepest sources of drinking water is not compromised. Analytical results from a monitoring well installed in the immediate vicinity of the Collier-Hogan 20-3H well and at the base of the deepest source of drinking water support the conclusion that impacts from hydraulic fracturing fluids have not migrated into the deepest sources of drinking water.

Key words: Hydraulic fracturing, Sunniland Formation, fluid migration.

1. Introduction

Interest in the environmental effects of hydraulic fracturing has become an increasingly important topic associated with the development of oil and natural gas because of the potential risk to the quality of shallow and deep aquifers. Although hydraulic fracturing has been in use since the 1960s, the ability of this technique to significantly enhance recovery of oil and natural gas from low permeability reservoirs and shale, has currently led to its widespread use in the U.S. and other petroleum-producing countries. Hydraulic fracturing is generally an environmentally safe practice because of the geologic conditions under which it is typically employed; however, in some instances hydraulic fracturing has been linked to inadvertent groundwater contamination and other health hazards, for example the fracturing of the Marcellus Shale in Pennsylvania for natural gas potentially resulted in groundwater contamination. In addition, the USGS (U.S. Geologic Survey) has also identified cases of hydraulic fracturing that have potentially resulted in environmental impacts. The USEPA (U.S. Environmental Protection Agency) [1] has summarized the development and potential adverse effects of hydraulic fracturing in a recent publication that identifies the most likely practices that result in groundwater contamination. The USEPA [1] concluded that impact to aquifers from the

Corresponding author: William C. Hutchings, Ph.D., senior hydrogeologist, research fields: flow and mass transport modeling.

injection of fluids into deep oil reservoirs, and subsequent migration, is not a known major source of groundwater contamination. Several other studies have evaluated the hydrogeologic conditions under which hydraulic fracturing takes place [2-5] and have also concluded that, in general, the vertical migration of injected fluids and natural gas to groundwater aquifers is unlikely [4, 5].

This research contributes to the understanding of the controls on fluid and potential contaminant migration, following high pressure hydraulic fracturing, with the use of the numerical model SEAWAT Version 4 [7] to simulate the hydrogeologic conditions and the effects of hydraulic fracturing in the Sunniland Formation of Southwest Florida. The Lower Cretaceous Sunniland Formation is an oil-producing trend within the South Florida Basin, half of which occurs within the onshore Florida peninsula [8]. The trend is approximately 145 miles (233 kilometers) long and 12 miles (19 kilometers) wide, extending from Sarasota to Dade counties. Production began in 1943, with the eventual discovery of 11 fields through 1984. To date, 120 million barrels have been produced from the formation. The Sunniland Formation occurs at a depth of approximately 12,000 feet (3,657 meters) below land surface, and is composed of 250 feet (76 meters) of limestone, dolomite and anhydrite. Exploration and production continue to date in the Sunniland Formation. A single instance of hydraulic fracturing took place at the Collier-Hogan 20-3H oil well located in Collier County (Fig. 1) in December 2013 that resulted in the immediate termination of further development of this well, due to unapproved extraction methods. To date, adverse effects associated with the migration of fracking fluids have never been documented in Florida. Although hydraulic fracturing has since been banned by numerous local governments, to date, the Florida legislature has not banned the practice.

This study is an assessment of the potential migration of the injected fluids from the reservoir associated with this event and variations of this event that include greater volumes of injectate and injection rates. The conclusions of this study could potentially apply outside of Southwest Florida to assess the behaviour of hydraulic fracturing fluids under generally similar hydrogeologic conditions. However, the hydrogeologic conditions under the Florida platform appear to provide several unique restrictions to the vertical migration of fluids from the Sunniland Formation to drinking water aquifers.

This paper is organized into the following sections: Introduction; Study Area; Hydraulic Fracturing Methods; Numerical Analysis; Results, Discussion; and Conclusions.

2. Study Area

The Sunniland Formation is a Lower Cretaceous sedimentary deposit composed of limestone, dolostone, and anhydrite [9]. The formation consists of an upper tidal shoal and a lower fractured carbonate oil play. Structural elements (Fig. 1) that occupy the Upper Sunniland formation include the Charlotte High, Lee-Collier Swell, and 40-Mile Bend High, from northwest to southeast. The formation is bounded by the Tampa-Sarasota Arch and the Peninsular Arch to the north, and the Pine Key Arch and Largo High to the south. The Florida Escarpment is located approximately 160 to 200 miles west of the Upper and Lower Sunniland formations, respectively. Only subtle structures with no major faults or vertical fractures have been identified onshore to date. However, in the offshore part of the basin, basement fault blocks and other complex structural features potentially exist, especially within the uppermost Jurassic and lowest Cretaceous part of the stratigraphic section [10]. The Sunniland Formation is not known to exhibit any major fractures/faults and was considered as a potential suitable formation for carbon dioxide-sequestration [11].

The general hydrogeology of Southwest Florida (Figs. 2a and 2b), from top to bottom, includes the

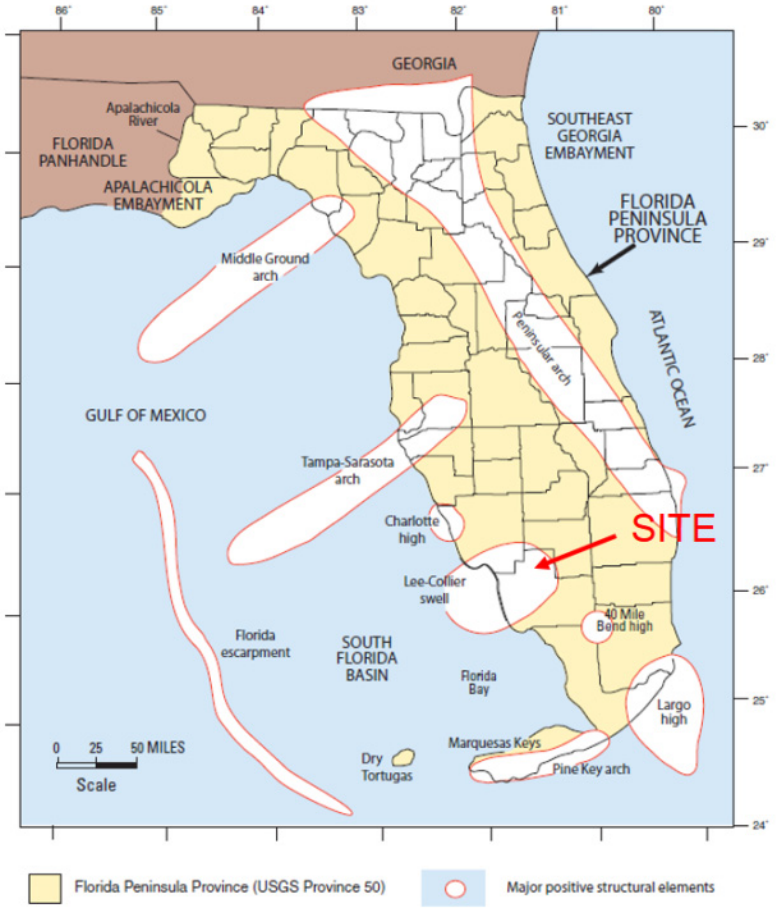

Fig. 1 Structural elements of the Florida Peninsula [6].

Series		Geologic Unit		Lithology	Hydrogeologic unit		Approximate thickness (feet)
HOLOCENE TO PLIOCENE		UNDIFFERENTIATED		Quartz sand, silt, clay, and shell	SURFICIAL AQUIFER SYSTEM	WATER-TABLE / BISCAYNE AQUIFER	20-300
		TAMIAMI FORMATION		Silt, sandy clay, micritic limestone, sandy, shelly limestone, calcareous sandstone, and quartz sand		CONFINING BEDS LOWER TAMIAMI AQUIFER	
MIOCENE AND LATE OLIGOCENE		HAWTHORN GROUP	PEACE RIVER FORMATION	Interbedded sand, silt, gravel, clay, carbonate, and phosphatic sand	INTERMEDIATE AQUIFER SYSTEM OR CONFINING UNIT	CONFINING UNIT SANDSTONE AQUIFER CONFINING UNIT MID-HAWTHORN AQUIFER CONFINING UNIT	250-750
			ARCADIA FORMATION	Sandy micritic limestone, marlstone, shell beds, dolomite,phosphatic sand and carbonate, sand, silt, and clay			
EARLY OLIGOCENE		SUWANNEE LIMESTONE		Fossiliferous, calcarenitic limestone	FLORIDAN AQUIFER SYSTEM	LOWER HAWTHORN PRODUCING ZONE UPPER FLORIDAN AQUIFER (UF) MIDDLE CONFINING UNIT MF LOWER FLORIDAN AQUIFER LF1 BZ	0-300 100-700 500-1,300 0-400 1,400-1,800 200-700
EOCENE	LATE	OCALA LIMESTONE		Chalky to fossiliferous, calcarenitic limestone			
	MIDDLE	AVON PARK FORMATION		Fine-grained, micritic to fossiliferous limestone, dolomitic limestone, dolostone, and anhydrite/ gypsum			
	EARLY	?	OLDSMAR FORMATION				
PALEOCENE		CEDAR KEYS FORMATION		Dolomite and dolomitic limestone			
				Massive anhydrite beds		SUB-FLORIDAN CONFINING UNIT	1,200?

Fig. 2a Stratigraphic and hydrogeologic column of SW Florida [16].

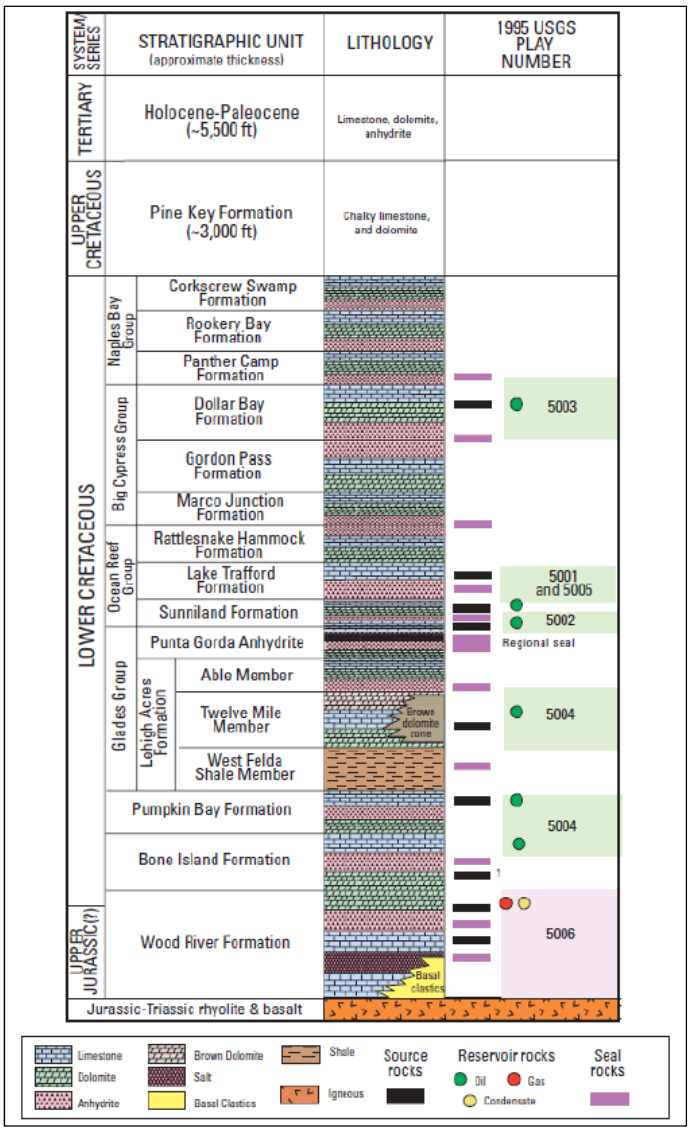

Fig. 2b Stratigraphic column of Southwest Florida [17].

Surficial Aquifer Systems (SAS) and Intermediate Aquifer Systems (IAS), extending to approximately 200 feet (61 meters) below land surface (ft bls), underlain by a confining unit and the underlying UFA (Upper Floridan Aquifer), at approximately 600 ft (183 m) bls, a sequence of Tertiary limestone. The SAS, including the water table aquifer and the Lower Tamiami aquifer, and IAS are the primary sources of drinking water in Southwest Florida. The middle confining unit separates the UFA from the LFA (Lower Floridan Aquifer). The LFA, at approximately 1,900 ft (579 m) bls, consists of micritic to fossiliferous limestone, dolomitic limestone, dolostone and anhydrite/gypsum. The Boulder Zone (BZ), at approximately 2,900 ft (884 m) bls, composed of highly fractured and cavernous dolomite, occurs in the Oldsmar Formation in the lower part of the LFA. The highly permeable BZ is approximately 400 ft (122 m) thick in the study area and is occupied by groundwater with seawater composition, supporting the theory of having a hydraulic connection to the Atlantic Ocean and Gulf of Mexico. According to the Kohout convection theory [12], seawater flows into the Lower Floridan aquifer BZ formation and, in response to the prevailing thermal gradient, flows vertically through the BZ and then flows laterally eastward into the

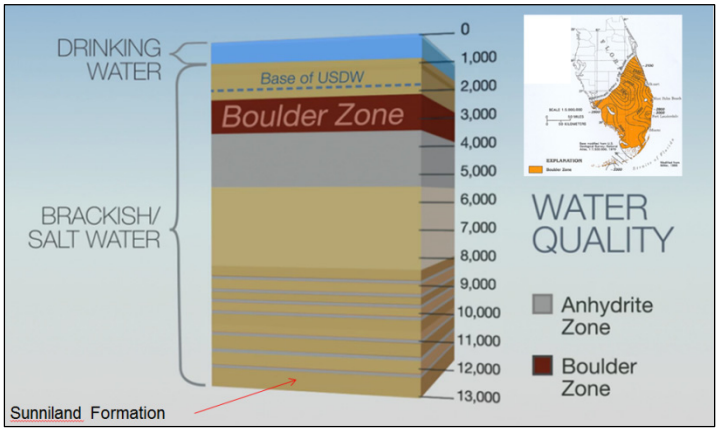

Fig. 3 Water quality characteristics underlying Southwest Florida.

Atlantic Ocean and westward into the Gulf of Mexico. The vertical distribution of drinking water and brackish water, BZ, and the base of the USDW (underground source of drinking water), identified by a TDS (total dissolved concentration) of 10,000 milligrams per liter (mg/L), are depicted on Fig. 3.

Underlying the LFA is the sub-Floridan confining unit consisting of Cretaceous to Upper Jurassic sediments composed of cyclic deposits of dolomite, limestone, and anhydrite. The Sunniland Formation occurs within this interval at a depth of approximately 12,000 ft (3,657 m) bls. The Upper Sunniland Formation is a tidal shoal deposit [6], which is the most productive oil reservoir in Southwest Florida. The Lower Sunniland Formation is known as a fractured dark carbonate oil play and has had only one productive well, which was installed in the Lake Trafford Field in 1969 [6].

The Collier-Hogan 20-3H well exhibits construction details in accordance with the Florida Department of Environmental Protection requirements including four cased intervals (Fig. 4) that serve to prevent migration of fluids within the borehole; thereby, protecting aquifers shallower than the base of the USDW. The general well construction details [13] include a 24-inch diameter conductor casing installed to a depth of approximately 250 ft (76 m) bls; 13-3/8-inch diameter surface casing set at 1,600 ft (488 m) near the bottom of the USDW; intermediate 9-5/8-inch diameter casing set at 3,850 ft (1,173 m) and cemented to the base of the Boulder Zone; and 4-1/2-inch diameter production casing set at 12,500 ft (3,810 m) with cement emplaced to 9,300 ft (2,835 m). Seven packers were installed in the horizontal section of the well between MTD (measured total depths) of 12,644 ft (3,854 m) and 16,215 ft (4,942 m) resulting in a fractured interval of 3571 ft (1,088 m). The TVD (true vertical depth) of the well is approximately 11,948 ft (3,642 m).

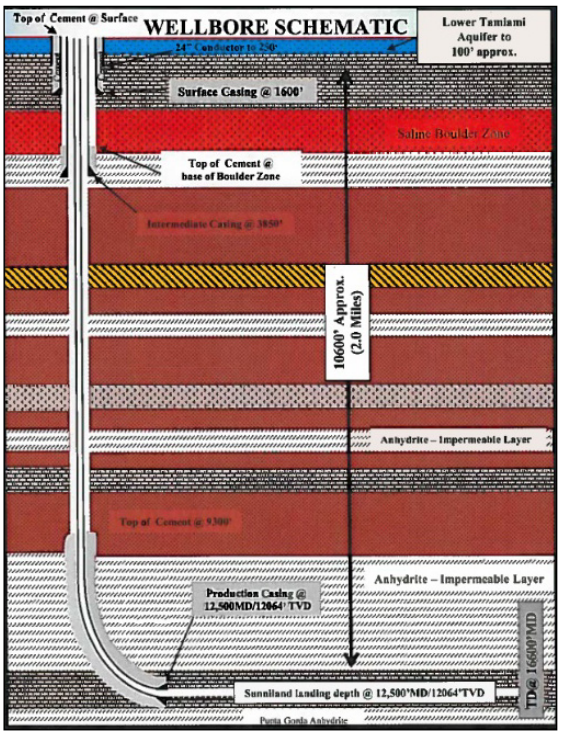

Fig. 4 Oil well construction details.

3. Hydraulic Fracturing Method

The orientation of fractures that develop in response to hydraulic fracturing is a function of the depth of the well and the distribution of the principal components of the stress field. Hydraulic fractures develop or propagate parallel to the principal vertical stress and open parallel to the direction of the least principal horizontal stress. In deep formations, i.e. greater than 2,000 ft, the vertical or overburden stress is greater than the horizontal stress; therefore, the fractures are vertically oriented. The hydraulic fracturing that was conducted at the Collier Hogan 20-3H well was designed with the MFrac3D Simulator by Baker Hughes [13] that predicted fractures 4.378 m (14.364 ft) above the lateral and 17.941 m (58.864 ft) below the lateral for a total of fracture height of 22.319 m (73.228 ft).

A total slurry volume of 691,068 gallons (16,454 barrels) that included 662,298 gallons of water and 637,399 pounds of proppant were used for the fracking treatment. On average, treatment pressures ranged from 8,287 to 8,397 pounds per square inch (psi) and the average injection rate per stage was 597 gallons per minute (gpm). The treatment was conducted in seven (7) stages with the injection time per stage equal to approximately 0.11 days, for a total treatment period of 2.09 days. The treatment procedure on the Collier-Hogan well was performed from December 30, 2013 to January 1, 2014.

4. Numerical Analysis

The SEAWAT Version 4.0 model was used to simulate the flow and mass transport characteristics associated with the natural system and hydraulic fracturing of the Sunniland reservoir in the vicinity of the Collier-Hogan 20-3H well. The SEAWAT model couples MODFLOW-2000 and MT3DMS. The MODFLOW-2000 code solves for the variable density flow field in terms of equivalent freshwater heads using the density determined from the MT3DMS-derived TDS concentrations present in each cell. This version of SEAWAT also includes the effects of salinity and temperature on viscosity, heat transport, and pressure on density. Given these recent modifications, SEAWAT is capable of simulating the hydraulic and geochemical conditions associated with this model.

4.1 Under-pressured and Over-pressured Scenarios

The finite difference grid for the three-dimensional model consisted of a horizontal domain with dimensions of 1005 by 520 meters discretized into 256 columns and 74 rows (Fig. 5). Model construction and parameter values are presented in Table 1. The model consisted of 52 layers (variable thicknesses) with constant head boundaries set up along the west and east sides of the model (Fig. 6). The north and south sides of the model were simulated as “no flow” boundaries. An expanding grid was used with rows and columns increasing from 3.05 meters in the vicinity of the horizontal injection well to 40 meters at the outer edges of the model. Row and column cell dimensions were maintained at 3.05 m in the vicinity of the horizontal well, determined from preliminary simulations, in order to accurately model fluid migration. Qualitative variations in the vertical distribution of hydraulic conductivities are illustrated in Fig. 7. The constant head boundaries ranged from 6.0 meters NGVD (National Geodetic Vertical Datum) for the water table to -710 meters in the Sunniland Formation for under-pressured conditions, based on measured formation pressures obtained from well construction records. A minor westward hydraulic gradient of 0.0001 was set up within each layer of the model. For over-pressured conditions, a hydraulic head of 6.0 meters was assigned to the Sunniland Formation. Due to historic production from the Sunniland Formation, the formation is currently under-pressured or less than the hydrostatic gradient [14]. TDS was assigned to the model, with 500 mg/L to the potable water of the surficial aquifer, 35,000 mg/L to the Boulder Zone, and 270,000 mg/L to the Sunniland Formation.

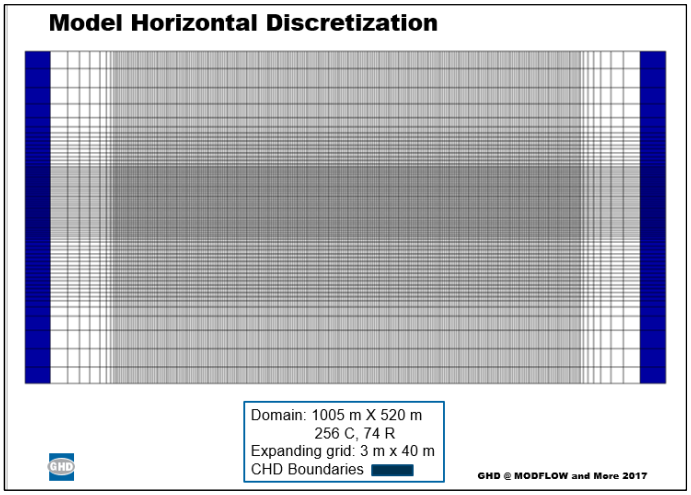

Fig. 5 Plan view of finite difference grid discretization.

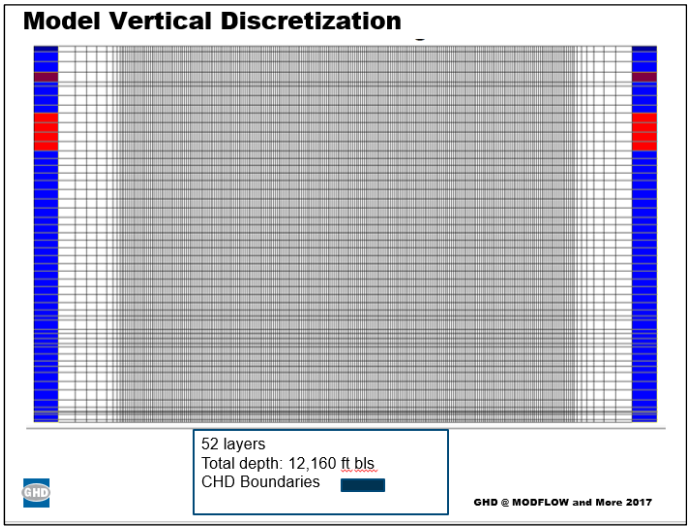

Fig. 6 Cross-sectional view of finite difference grid discretization.

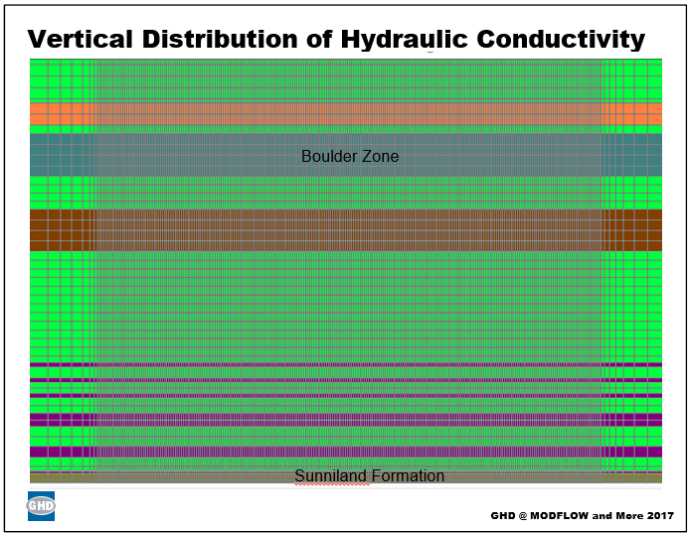

Fig. 7 Model cross-sectional view of hydraulic conductivity distribution.

Table 1 Model construction and input parameter values.

Input parameters	Units	Values
Number of columns (NCOL)		256
Number of rows (NROW)		74
Number of layers (NLAY)		52
Δx (DELR)	m	3.05 to 40
Δy (DELC)	m	3.05 to 40
Δz (DZ)	m	7 to 100
Horizontal hydraulic conductivity (Kh)-anhydrite	m/d	3.32E-05
Vertical hydraulic conductivity Kv)-anhydrite	m/d	3.32E-05
Horizontal hydraulic conductivity (Kh)-limestone	m/d	2.80E+01
Vertical hydraulic conductivity Kv)-limestone	m/d	2.80E+01
Horizontal hydraulic conductivity (Kh)-Sunniland Fm	m/d	8.30E-01
Vertical hydraulic conductivity Kv)-Sunniland Fm	m/d	8.30E-01
Horizontal hydraulic conductivity (Kh)-Boulder Zone	m/d	5.54E+03
Vertical hydraulic conductivity Kv)-Boulder Zone	m/d	5.54E+03
Horizontal hydraulic conductivity (Kh)-Cedar Keys	m/d	1.40E-04
Vertical hydraulic conductivity Kv)-Cedar Keys	m/d	1.40E-04
Horizontal hydraulic conductivity (Kh)-Avon Park	m/d	1.10E-01
Vertical hydraulic conductivity Kv)-Avon Park	m/d	1.10E-01
Horizontal hydraulic conductivity (Kh)-Fracture	m/d	2.80E+02
Vertical hydraulic conductivity Kv)-Fracture	m/d	2.80E+02
Specific storage (Ss)	m^{-1}	1e-4 to 1e-6
Porosity (θ)	ND	0.2 to 0.35
Longitudinal dispersivity (αL)	m	1
Transverse dispersivity (αT)	m	0.1
Heat capacity of the solid (CPsolid)	J/(kg°C)	835
Density of the solid (ps)	kg/m^3	2710
Bulk density (pb)	kg/m^3	1761
Thermal conductivity of solid (kTsolid)	W/(m°C)	3.59
Bulk thermal conductivity (kTbulk)	W/(m°C)	2.547
Diffusion coefficient (Dm_salinity)	m^2/d	1.00E-10
Bulk thermal diffusivity (Dm_temp)	m^2/d	0.150309621
Heat capacity of the fluid (CPfluid)	J/(kg°C)	4183
Thermal conductivity of water (kTfluid)	W/(m°C)	0.61
Distribution coefficient for salinity (Kd_salinity)	m^3/kg	0
Distribution coefficient for temperature (Kd_temp)	m^3/kg	2.00E-04
Reference density (ρ_0)	kg/m^3	1000
ōρ/ōC		0.7
Reference concentration for density ($C\rho_0$)	kg/m^3	0.5
ōρ/ōT		-0.375
Reference temperature (T_0)	°C	24
Temperature range	°C	24 to 100
Temperature gradient	°C/km	20.5
Reference viscosity	Kg/(ms)	0.001
ōμ/ōC	m^2/d	1.92E-06
Reference concentration for viscosity (Cμ0)	kg/m^3	0.5
ōρ/ōP	kg/m^4	4.46E-03
TDS	kg/m^3	0.5-275

Representative values of TDS were assigned to the Floridan aquifer and a linear gradient was used between the Boulder Zone and the Sunniland Formation. Temperatures ranged from 24 to 100 degrees centigrade, with a gradient of 20.5 °C/kilometer assigned to the model.

Density ranged from 1,000 to 1,181 kg/m^3 ($\delta\rho/\delta T$ -2.40 kg/(m^3 ºC). Viscosity varied throughout the model according to $\delta\mu/\delta C = 1.92 \times 10^{-6}$ m^2/d. Density and salinity varied according to the relationship, $\delta\rho/\delta C = 0.7$. The density-pressure slope was set at 4.46E^{-3} kgm^4. Hydraulic conductivities were assigned to the models as: anhydrite - 3.3240E^{-5} m/day; limestone/dolostone - 2.8E^{+1} m/day; Sunniland Formation - 8.3E^{-1} m/day (pre-fracture); > 8.3 m/day (post-fracture); Boulder Zone dolomite - 5.54E^{+3} m/day; Cedar Keys Formation -1.4E^{-4} m/day; Avon Park Formation - 1.1E^{-1} m/day; and fault/fracture - 280 m/day. The diffusion coefficient was set at 1E^{-10} m^2/day. Specific storage ranged from 1E^{-4} to 1E^{-6} per meter and porosity ranged from 0.35 to 0.2. All other terms and values used in the models are consistent with this type application of the model and can be found in the SEAWAT model documentation [7].

The simulated hydraulically fractured zone was assigned to layer 52 with a length of 545 meters, width of 15.25 meters, and depth of 23 meters (Fig. 8). The modeled horizontal well length is approximately half of the Collier Hogan 20-3H, which should amplify the potential effects of plume injection and migration. Modelling the decreased well length significantly reduces simulation run times, without adversely affecting the modelling results. The base case simulation represents under-pressured conditions with fluid injection rates that are consistent with the hydraulic fracturing event. An additional simulation representing over-pressured conditions was run with similar injection rates over the hydraulic fracturing period. Since hydraulic fracturing can be performed using higher volumes of injectate, additional simulations were run representing under and over-pressured conditions with injection rates two and four times the base case simulation. TDS is used in the models as a tracer to track and evaluate potential plume migration. Injection was simulated with pumping wells set up in 175 cells injecting 136 m3/day (base case), 272 m3/day (2 x base case) and 544 m3/day (4 x base case) to identify the potential differences in migration characteristics. The total volumes injected during the three previous scenarios are 662,298 gallons (2,506,798 liters), 1,324,596 gallons (5,013,596 liters, and 2,649,192 gallons (10,027,192 liters) respectively. A potential vertical fracture/fault (3.05 × 3.05 m) extending from layer 51 to layer 37 was then set above the center of the horizontal well to simulate a hypothetical anomalous hydraulic preferential pathway. Hydraulic conductivity of this preferential flow path was set at 280 m^3/day, which is consistent with faults [4]. Backflow was simulated at 30% of the injected volume to occur over 30 days and production was simulated at 160 barrels per day for 10 years into the future, which was anticipated and consistent with production in the formation.

The flow system was solved using the Pre-conditioned Conjugate Gradient Package. The advection component of the transport equation was solved using the Total-Variation Diminishing option. Dispersion, reaction and sources/sinks terms were solved using the Generalized Conjugate Gradient solver with the Slice-Successive Over-relaxation Package for pre-conditioning. Seven equal sections of the horizontal well were sequentially assigned 0.11 days of injection followed by 0.22 days of inactivity representing the first 13 stress periods. Subsequently, the models were run for an additional 107 stress periods of 30 days each, for a total of 120 stress periods.

5. Results and Discussion

The model simulation exhibiting the initial flow system and TDS distribution (Fig. 9) is consistent with the distribution of constant head and concentration

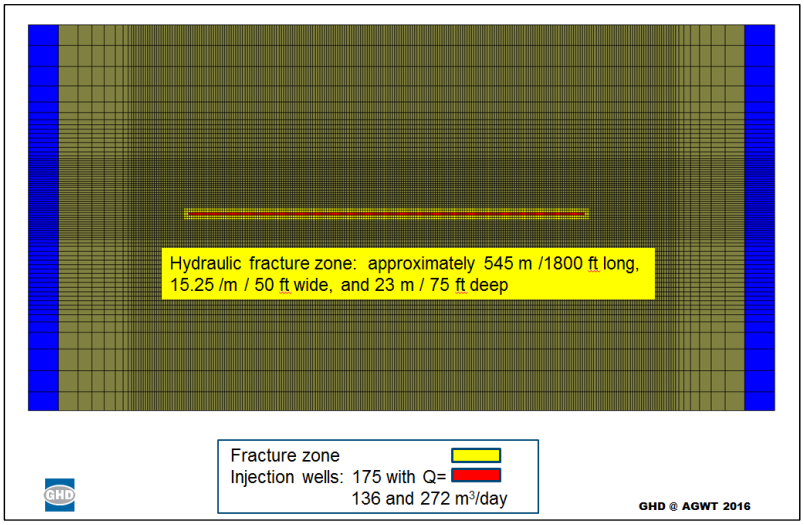

Fig. 8 Horizontal discretization, horizontal well and hydraulic fracture zone configuration.

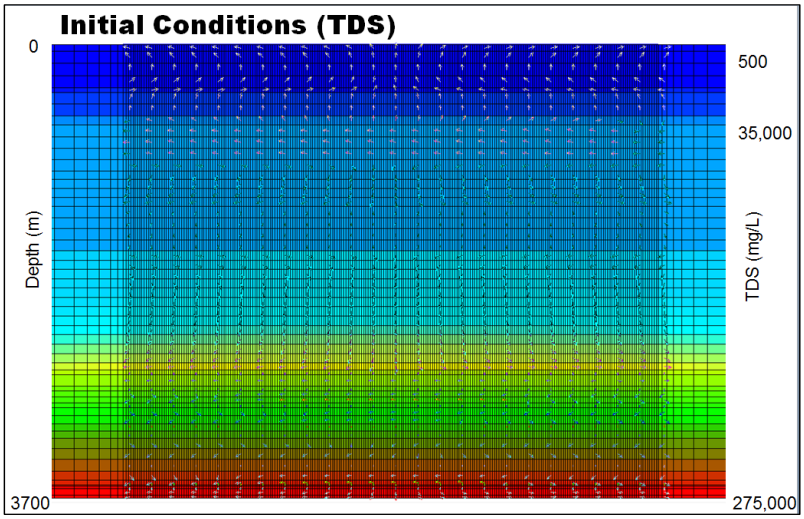

Fig. 9 Initial TDS conditions and flow system.

boundaries, depicting upward flow in the Floridan aquifer, horizontal flow in the Boulder Zone, and downward flow between the Boulder Zone and the Sunniland Formation.

The hydraulic head distribution of the base case model (without a fracture/fault) after stage 7 of the injection period exhibits a significant increase in head (approximately 400 m), which is generally restricted to the near vicinity of the horizontal well (Fig. 10).

The TDS distribution after stage 7 in this same simulation exhibits a decrease in TDS concentration in the immediate vicinity of the horizontal well, due to the injectate fluid, with lateral migration restricted to the permeable zone created by the hydraulic fracturing and no vertical migration. The hydraulic head distribution of the model (with a fracture or fault) after stage 7 of the injection period (Fig. 11) shows a similar increase in head (approximately 400 m) compared to the base case simulation. After 90 days, the TDS concentration in the area affected by the rising plume is approximately 207 mg/L and, after 360 days, the TDS concentration has increased to 225 mg/L and the diameter of the impacted area has also increased. In layer 47 of this simulation, it is evident that the injectate has migrated to this layer after 90 days by the range of TDS concentrations, 231 to 254 mg/L. After

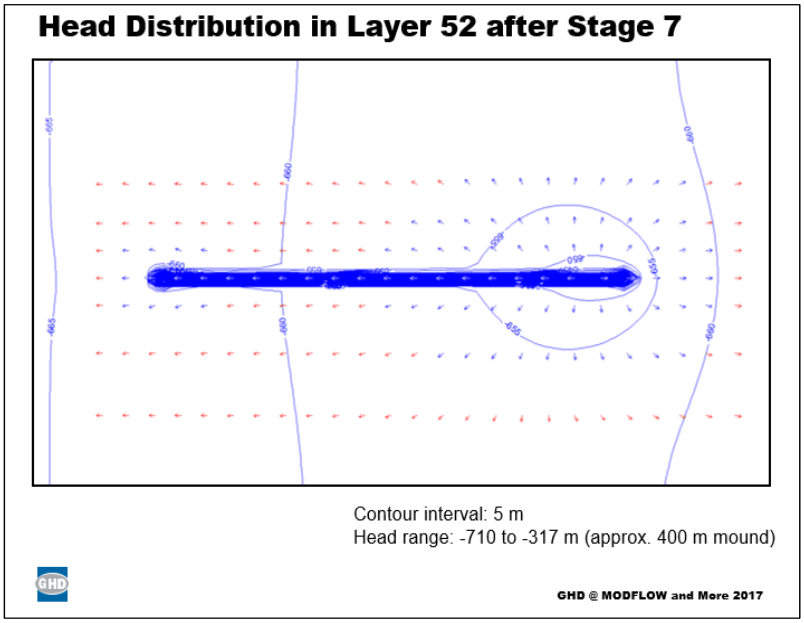

Fig. 10 Hydraulic head distribution in layer 52 after stage 7.

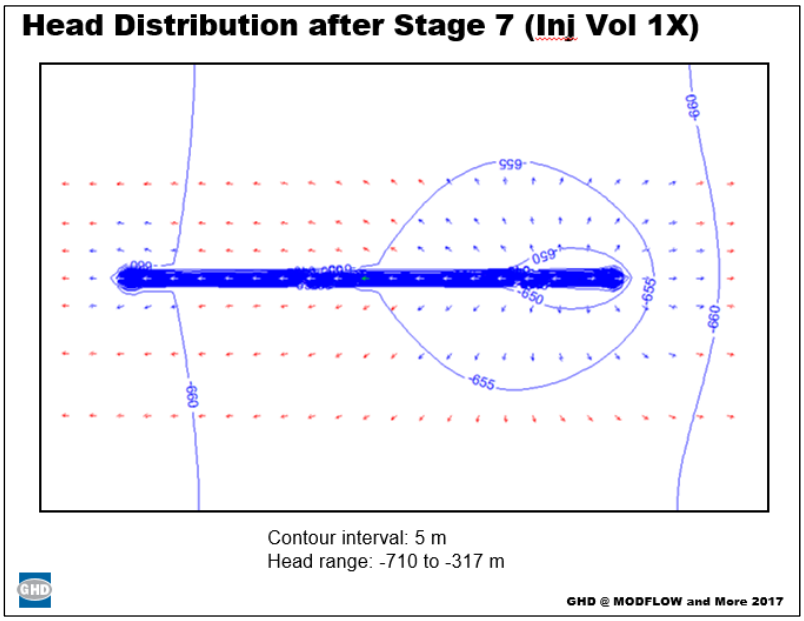

Fig. 11 Hydraulic head distribution in layer 52 after stage 7 (with fracture/fault).

360 days, the range of TDS concentrations has generally decreased from 194 to 229, in the vicinity of the ascending plume. The vertical extent of the plume extends to layer 44 with a plume exhibiting TDS ranging from 225 to 257 mg/L.

The distribution of TDS after 360 days exhibits the maximum vertical extent of the injected plume in layer 44 for both (base case and 2x) under-pressured conditions, a vertical distance of approximately 460 meters. The plume continues to migrate horizontally, although vertical migration has essentially ceased. The vertical and lateral distributions of TDS in the model are exhibited in Fig. 12 and 12a. These figures exhibit the vertical and lateral migration of the plume, with the largest plume diameter shown in layer 44. The increased plume diameter in layer 44 is likely due to

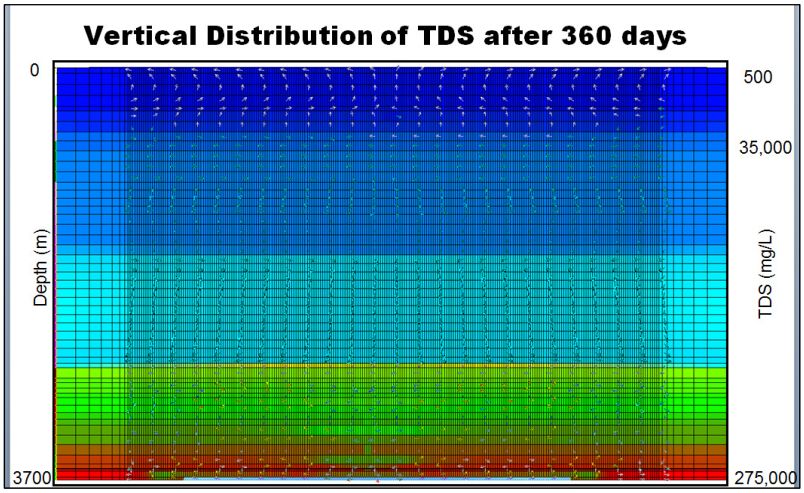

Fig. 12 TDS distribution after 360 days showing the vertical extent of injected fluids plume in layer 44.

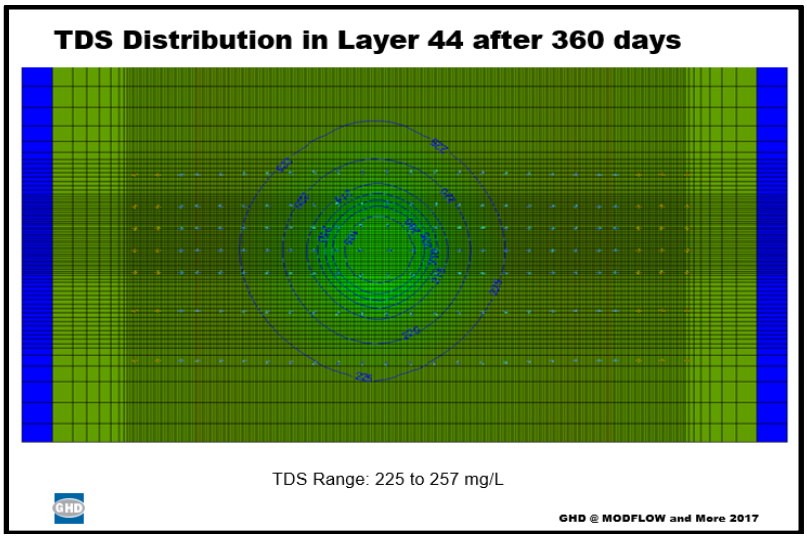

Fig. 12a TDS distribution after 360 days showing the lateral distribution of injected fluids plume in layer 44.

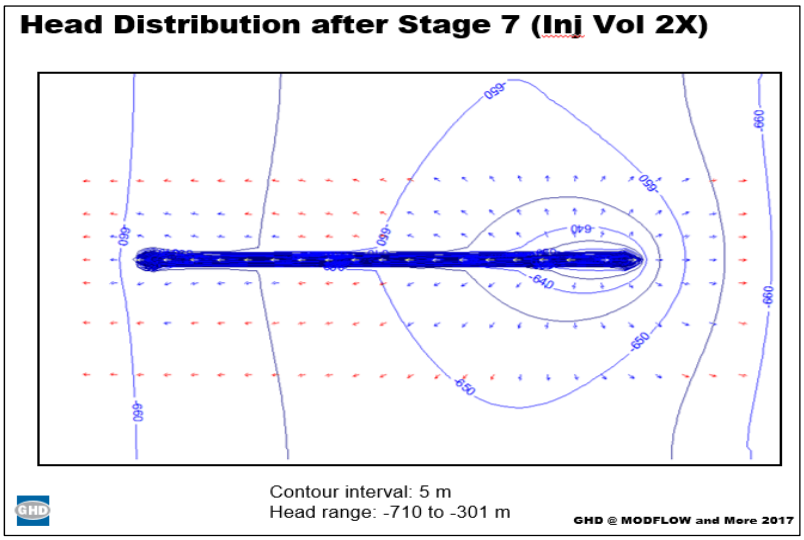

Fig. 13 Hydraulic head distribution in layer 52 after stage 7 (with fracture/fault and injection volume 2x).

spreading in response to advection related to the residual pressure field soon after injection; however, late time migration is likely due to the hydraulic gradient.

The hydraulic head distribution of the model (with a fracture/fault), with injection twice the base case model, after stage 7 of the injection period shows that increase in head (approximately 409 m) exhibits a greater head (by approximately 10 m) and head distribution around the horizontal well, compared to the distribution using half of the injection rate (Fig. 13). The cross-sectional TDS distributions after 360 (Fig. 14) and 720 days are generally similar to those exhibited by the base case models with a fracture/fault, with increased spreading due to the additional volume of injected fluid. The vertical extent of plume migration generally occurs in layer 44, which is a distance of approximately 460 m, although minor migration into layer 42 is evident.

The hydraulic head distribution of the model (with a fracture/fault), with an injection volume four times the base case model (Fig.15), after stage 7 of the injection period exhibits a maximum head difference

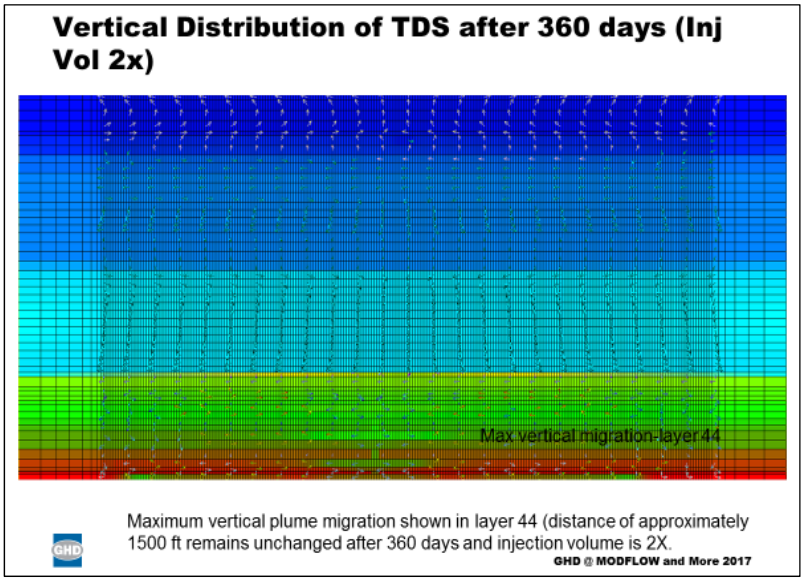

Fig. 14 TDS distribution after 360 days showing the vertical extent of injected fluids plume in layer 44 (with fracture/fault and injection volume 2x).

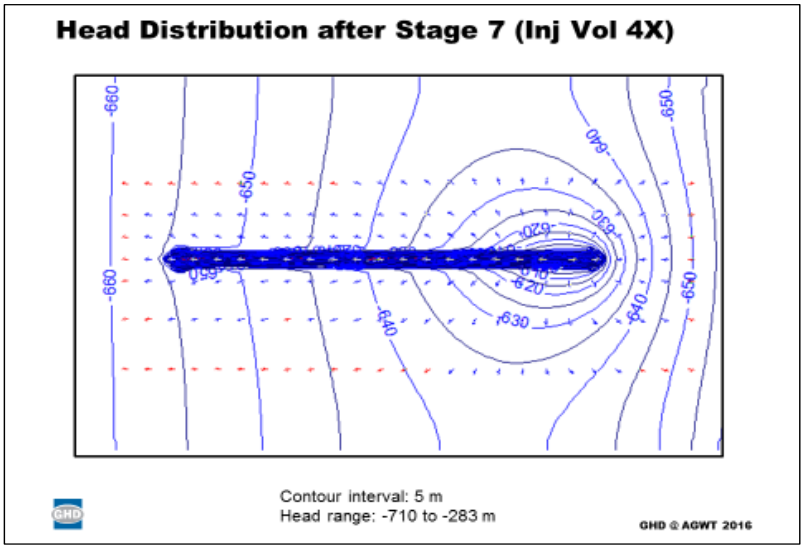

Fig. 15 Hydraulic head distribution in layer 52 after stage 7 (under-pressured with fracture/fault and injection volume 4x).

of 427 m. The TDS distribution is generally similar to the preceding scenario using under-pressured conditions and twice the base case injection rate after seven years, with the exception that the amount of fluids that migrate is greater, as exhibited by Fig. 16. Although most of the mass resides between model layers 52 and 44, minor evidence of migration indicates that the plume has broken through to layer 42.

The hydraulic head distribution of the model (with a fracture/fault), with injection twice the base case model, and under over-pressured conditions, after stage 7 of the injection period (Fig. 17) exhibits hydraulic heads ranging from -70 to 270 m, a difference of 340 m. In this scenario, the heads are distributed about the centrally-located fracture/fault instead of the east end of the well, which is the location of the last stage of the hydraulic fracturing event. Apparently, the fracture is an opening to the

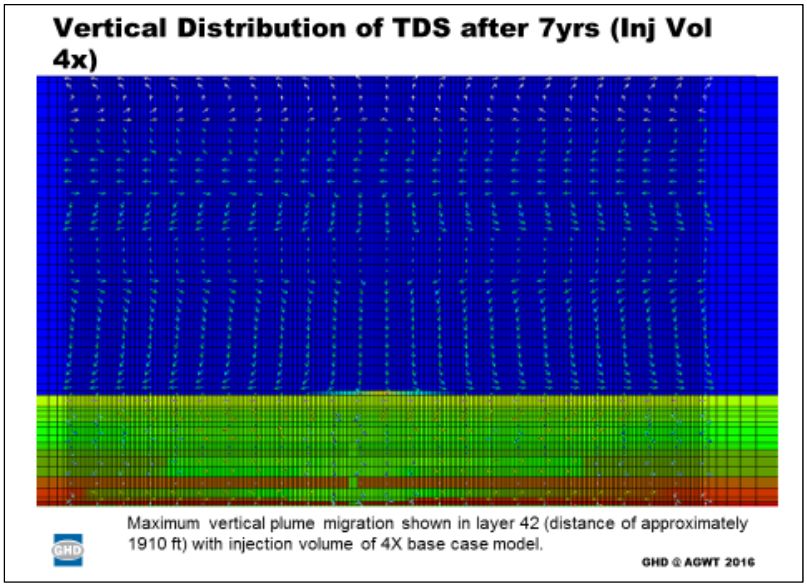

Fig. 16 TDS distribution after 7 years showing the vertical extent of injected fluids plume in layer 44 ((with fracture/fault and injection volume 4x).

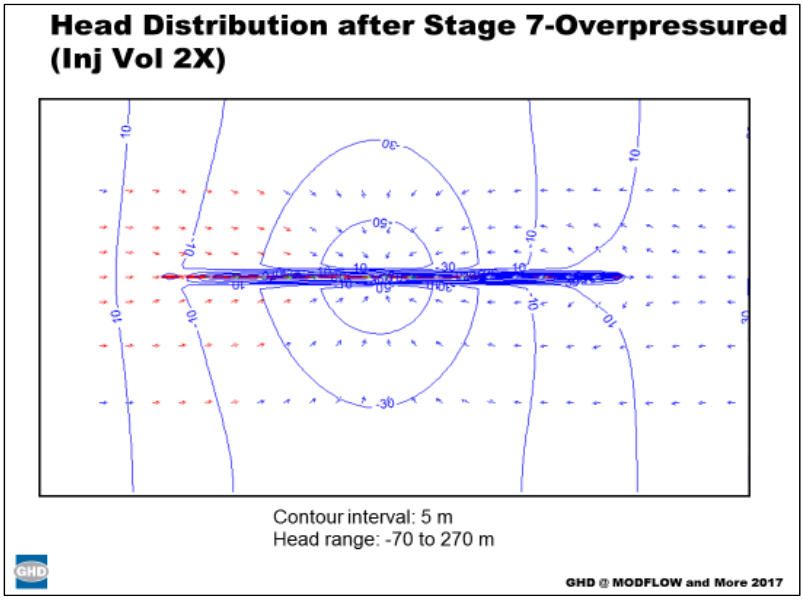

Fig. 17 Hydraulic head distribution in layer 52 after stage 7 (over-pressured with fracture/fault and injection volume 2x).

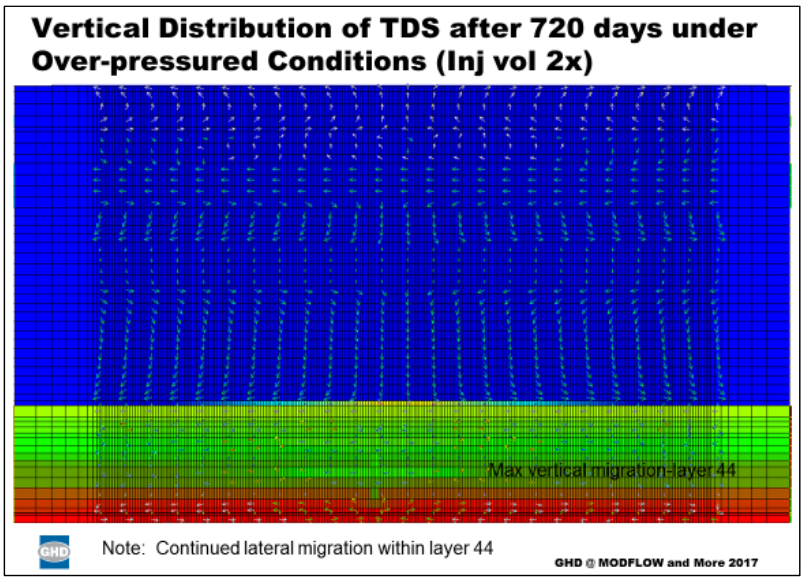

Fig. 18 TDS distribution after 720 days showing the vertical extent of injected fluids plume in layer 44 (over-pressured with fracture/fault and injection volume 2x).

very low formation pressure of layer 51 causing a hydraulic sink and the injected fluids to migrate to this low-pressure part of the well. The vertical distribution of TDS through time after 90, 360 and 720 days is generally similar to the preceding scenario using under-pressured conditions and twice the base case injection rate, where the vertical extent of the plume generally occurs in layer 44.

The results of these simulations consistently exhibit several similarities, regardless of the operating conditions associated with the hydraulic fracturing scenarios. The hydraulic heads generated during the hydraulic fracturing simulations are approximately 400 m for under-pressured conditions and 340 m for over-pressured conditions. This head difference appears to be the result of the difference in pressure of the high-density reservoir water column associated with each scenario, i.e. under over-pressured conditions the water column is approximately 12,000 ft (3,657 m). In all of the simulations, the lateral head distributions exhibit very high horizontal hydraulic gradients indicating that the high fracturing pressures are generally restricted to the immediate vicinity of the fractured zone. Another consistency is the TDS concentration distributions in the reservoir following hydraulic fracturing. Similar to the head distributions, all of the simulations exhibit variations in TDS concentrations that occur in the immediate vicinity of the fractured zone with background TDS concentrations occurring immediately beyond the fractured zone after hydraulic fracturing. With increasing time to approximately greater than seven years, the TDS plume grows beyond the fractured zone in the vicinity of the fracture/fault, as fluids migrate to the fault. Beyond the vicinity of the fracture/fault, the TDS plume does not migrate far from the fractured zone. The rapid reduction in the pressure field and TDS distribution beyond the fractured zone is generally attributed to fracture mechanics, losses to the formation (leak off), and backflow, which was set at 30% of the injection volumes for all of the models and simulations. The fracture length is determined by the mass balance between leakoff and flow into the fracture [15]. The vertical extent of fluid migration in all cases generally terminates at model layer 44, which is equivalent to a distance of approximately 460 m, beyond which lateral spreading is dominant. With increasing injection volumes, the volume of fluids that migrate from the injection zone into the overlying formations increases with most of the mass generally maintained in model layers deeper than layer 44, although the results do indicate some migration into

layer 42. Since TDS was used as a tracer to track fluid migration and the constituents of the plume, these modeling results indicate that any regulated constituents in the plume will not migrate beyond the distance attained by the TDS plume.

When evaluating the potential effects of injecting the volumes of fluid for these various scenarios, it should be considered that the volumes are distributed over a model distance of 545 meters. The actual length of the horizontal well is approximately twice this length or 1,090 meters (3,576 feet). Therefore, a significantly larger volume of the injectate is in contact with reservoir brine with a TDS concentration of 270,000 mg/L, compared to a vertical well used for ASR (Aquifer Storage Recovery) that would potentially have the base case volume injected into a few hundred feet of the Floridan aquifer, eventually creating a freshwater zone about the injection zone. Prior to creating the freshwater zone in a brackish formation used for ASR, much water is lost to the formation. Similarly, much of the low TDS injected water used for hydraulic fracturing should rapidly experience an increase in TDS resulting in reduced buoyancy.

6. Conclusions

This study, based on the application of a numerical model incorporating site-specific hydrogeologic and fluid injection parameters, demonstrates that the injected fluid from hydraulic fracturing does not have the potential to migrate into the USDW (Underground Source of Drinking Water) that occurs in the Lower Floridan aquifer. The vertical migration of the injected solution is restricted from migrating into drinking water aquifers as a result of the following conditions:

- the presence of low permeability formations composed of clay, anhydrite, limestone and dolomite overlying the reservoir;
- very high salinities and increasing density with depth;
- downward hydraulic gradient associated with under-pressured conditions;
- general absence of naturally occurring faults in the Sunniland Formation and sub-Floridan confining unit;
- without a fracture or fault exhibiting a preferential flow path, vertical migration from the reservoir does not occur;
- with presence of a fracture/fault, vertical migration is limited to approximately 460 meters;
- presence of the Boulder Zone and associated Kohout convection, potentially restricts migration into the USDW;
- horizontal plume migration is restricted to near vicinity of the hydraulic fracture zone.

The deep monitoring well installed at the base of the USDW, in the vicinity of the Collier-Hogan 20-3H oil well, has not exhibited any impacts related to the injected fluids to date, supporting the conclusion that such fluids are not capable of migrating through the various hydrogeological barriers between the reservoir and the USDW over the short periods of high pressure hydraulic fracturing events or longer periods of post fracturing residual migration due to buoyancy of the injected fluids. These results are in agreement with the general conclusion, based on an extensive body of evidence compiled by the USEPA, that impacts to aquifers have not been found to result from the migration of the fluids associated with hydraulic fracturing of deep formations.

References

[1] USEPA (U.S. Environmental Protection Agency). 2016. Hydraulic Fracturing for Oil and Gas: Impacts from the Hydraulic Fracturing Water Cycle on Drinking Water Resources in the United States. Final report of EPA-600-R-16-236Fa, Office of Research and Development, Washington, DC..

[2] Meyer, T. 2012. “Potential Contaminant Pathways from Hydraulically Fractured Shale to Aquifers.” *Groundwater* 50 (6):872-82.

[3] Hsieh, P. A. 2011. “Application of MODFLOW for Oil Reservoir Simulation during the Deepwater Horizon Crisis.” *Groundwater* 49 (3): 319-23.

[4] Birdsell, D. T., Rajaram, H., Dempsey, D., and Viswanathan, H. S. 2015. “Hydraulic Fracturing Fluid

Migration in the Subsurface: A Review and Expanded Modeling Results." *Water Resources Research* 51: 7159-88. doi: 10.1002/2015WRO17810.

[5] Flewelling, A. S., and Sharma, M. 2014. "Constraints on Upward Migration of Hydraulic Fracturing Fluid and Brine." *Groundwater* 52 (1): 5-19.

[6] Pollastro, R. M. 2001. "1995 USGS National Oil and Gas Play-Based Assessment of the South Florida Basin, Florida Peninsula Province." In US Geological Survey Digital Data Series 69-A. Virginia: U.S. Geological Survey, 17.

[7] Langevin, C. D., Thorne Jr., D. T., Dausman, A. M., Sukop, M. C., and Guo, W. 2007. "SEAWAT Version 4: A Computer Program for Simulation of Multi-species Solute and Heat Transport." In U.S. Geological Survey Techniques and Methods, Chapter A22, 39. Virginia: U.S. Geological Survey.

[8] Applegate, A. V., and Pontigo Jr., F. A. 1984. Stratigraphy and Oil Potential of the Lower Cretaceous Sunniland Formation in South Florida. Report of Investigation No. 89, Florida Department of Natural Resources, Division of Resource Management. Tallahassee: Bureau of Geology.

[9] Mitchell-Tapping, H. J. 2003. "Exploration of the Sunniland Formation of Southern Florida." AAPG Search and Discover Article #90021, presented in GCAGS 53rd Annual Convention, Baton Rouge, Louisiana.

[10] Pollastro, R. M., Schenk, C. J., and Charpentier, R. R. 2001. "Assessment of Undiscovered Oil and Gas in the Onshore and State Waters Portion of the South Florida Basin, Florida-USGS Province 50." In US Geological Survey Digital Data Series 69-A. Virginia: US Geological Survey, 70.

[11] Ashby, T. R. 2010. "Evaluation of Deep Geologic Units in Florida for Potential Use in Carbon Dioxide Sequestration." Ph.D. thesis, University of South Florida.

[12] Meyer, F.W. 1989. *Subsurface Storage of Liquids in the Floridan Aquifer System in South Florida.* Open File Report 88-47, U.S. Geological Survey. Tallahassee, Florida.

[13] Arthur, J. D. 2014. Expert Evaluation of the D.A. Hughes Collier-Hogan 20-3H Well Drilling and Workover. Tulsa: ALL Consulting, LLC.

[14] Burke, L. A., Kinney, S. A., Dubiel, R. F., and Pitman, J. K. 2012. "Regional Map of the 0.70 psi/t Pressure Gradient and Development of the Regional Geopressure-gradient Model for the Onshore and Offshore Gulf of Mexico Basin, U.S.A." *Gulf Coast Association of Geological Societies* 1: 97-106.

[15] Xavier, N. F. 2013. "Control of Height Growth in Hydraulic Fracturing." A Paper of Dalhousie University. Halifax: Dalhousie University.

[16] Reese, R.S. 2000. "Hydrogeology and the Distribution of Salinity in the Floridan Aquifer System, Southwestern Florida" U.S. Geological Survey Water Resources Investigations Report, 98-4253 (2000), 11.

[17] Pollastro, R. M. "1995 USGS National Oil and Gas Play-Based Assessment of the South Florida Basin, Florida Peninsula Province." Chapter 2 of National Assessment of Oil and Gas Project: Petroleum Systems and Assessment of the South Florida Basin, compiled by Richard M. Pollastro and Christopher J. Schenk, U.S. Geological Survey Digital Data Series 69-A (November 2001), Figure 2, page 3.

Journal of Environmental Science and Engineering A 7 (2018) 125-131
doi:10.17265/2162-5298/2018.03.003

Characterization of Ultrasonic Metal Welding Process

Sandra Matos[1], Fernando Veloso[2], Carlos Santos[2], Leonardo Gonçalves[3] and Emanuel Carvalho[4]

1. Department of Polymers, University of Minho, Guimarães 4800-058, Portugal

2. Engineering Department, Aptiv, Lisbon 1600-514, Portugal

3. Polytechnic Institute of Setubal, Setubal 2910-761, Portugal

4. Superior Institute of Engineering, Lisbon 1959-007, Portugal

Abstract: The ultrasonic welding process for wires is being largely used on industry mainly on applications that involve the connection between similar or different metals. The biggest benefit of this technology is the possibility to perform the weld without addition materials, like terminals, metal rings or tapes. Manufacturing of wiring harnesses demands a significant amount of joining, such as welding, crimping or soldering, to fulfill the desired layout of the harnesses and capacity requirements, but conventional connection processes, face difficulties in joining multiple cross sections mainly due to the characteristics of the processes and equipment in use. Ultrasonic metal welding process overcomes these issues due to the solid-state characteristics inherent to the process itself that include the excellent electrical properties of the joint. Several researches on ultrasonic metal welding are being done to define the fundamental mechanisms behind this process and it is being seen that they are completely dependent on the cross section to be welded. With this research we are trying to develop methods for process characterization and define acceptable quality parameters in this process. The main topics addressed in this paper are the characterization the weld formation using copper-to-copper wires using optical microscopy and the analysis of insulation material when submitted to different thermal conditions.

Key words: Ultrasonic metal welding, wiring harnesses, insulated wires, splices, harness assemblies, PVC (Polyvinyl Chloride).

1. Introduction

Ultrasonic metal welding was discovered around 1950 and is now widely used on the industry in applications that involve softer and high conductivity alloys or metals like copper or aluminum [1, 2]. The metal joint is formed by the application of high frequency vibrations and moderate pressure. The application of vibrations is done parallel to the interface of the parts [3] and the applied frequency creates some motion between the parts to be welded that forms the solid-state weld by plastic deformation and progressive shearing of the metal that should disperse oxides or contaminates over the asperities, creating a clean area of metal contact [3]. The equipment used to perform the ultrasonic welding should be able to control welding variables and monitor energy and consequently solve oxidation problems, high electrical and thermal conductivity [4]. The process overcomes easily the difficulties of multiple cross-sections connection due to its solid-state characteristics that creates a true metallurgical bond [5, 6]. Also, the temperature of the process does not exceed the melting point of the material which eliminates undesirable compounds and metallurgical defects that can be seen on other types of welding [7].

The ultrasonic welding process consists of the conversion of electrical into mechanical vibrations using a frequency of 20 to 40 kHz and the system should include a generator, a converter with piezoelectric ceramics, a booster and a sonotrode as shown in Fig. 1 [8].

Ultrasonic metal welding process is known for many years [3] but when considering the welding of copper insulated wires there seems to exist a lack of understanding of the welding mechanisms that should be known for a number of years, mainly when considering wires insulated with PVC (Polyvinyl Chloride).

Corresponding author: Sandra Matos, Ph.D. student, main research field: polymers.

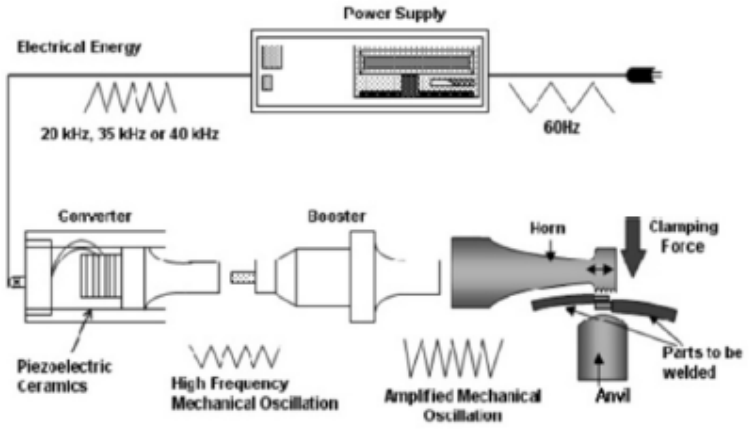

Fig. 1 Schematic of ultrasonic welding process [8].

Several researches are being done in order to determine the influence of the insulation materials on the welding process of wires. This study was focused mainly in two distinct areas: (1) the characterization of the weld formation of copper-to-copper wires using optical microscopy and (2) the analysis of insulation material when submitted to different thermal conditions. As mentioned, there were many studies already done on this topic but are mainly focused on material thickness, in the specific case of electrical wires the main issue is related to cross section to be welded and the sticking of material to the tooling [3], and the second issue is totally dependent on the type of insulation material used on copper wires.

2. Methods and Materials

Ultrasonic welding splices can be created in two different ways, one with all wires in the same side and second with wires distributed by both sides of the splice [8] as shown in Fig. 2.

For characterization of weld formation test samples were created with wires in one side using ultrasonic welding machine for splices [9] and the evaluation of characteristics of weld formation was done using electronic microscopic techniques.

Evaluation of the weld ability was checked by the results on the strength force measurement needed to break the connection between wires. A capability study (Eq. (1)) using the strength needed to remove one wire from the splice was done.

$$Ppk = \frac{\mu - LSL}{6\sigma} \quad (1)$$

To evaluate the characteristics of the insulation material, samples were created by removing 50 mm of insulation from the electrical wire. To check if there is influence of insulation material on welds formation cables with two types of insulation were chosen, PVC as it is known that may cause negative effect on the welding process and ETFE (Ethylene Tetrafluoroethylene) that seems to have no impact on the weld formation.

According to automotive standard LV112 [10] samples should be analyzed by infrared spectroscopy technique to identify if degradation of materials exists and FTIR (Fourier-Transform Infrared Spectroscopy) was the method chosen as it is a faster technique to collect the infrared spectrum and technique main advantage is that all the radiation emitted by the source is continuously monitored [11]. In this specific case the material was analyzed on three different temperatures, RT (room temperature), 40 ºC and 70 ºC.

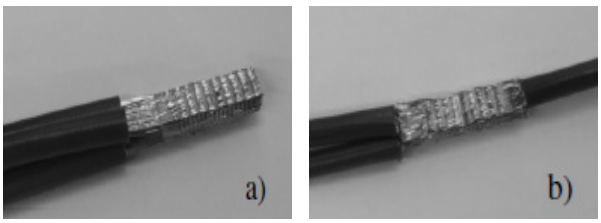

Fig. 2 Splice with all wires on one side (a) and both sides (b).

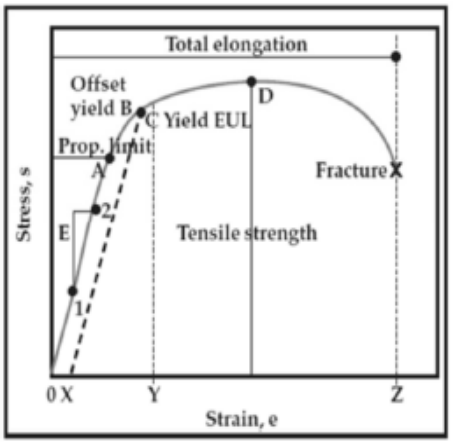

Fig. 3 Diagram stress vs. strain [13].

The tensile strength of a material (maximum force required to draw the material to break) refers to the ability of the material to withstand loads without failure due to excessive stresses or deformations. According to automotive standards, DIN EN 60811-1-1 [12] and LV112 [10], this test is also used to evaluate material degradation.

The tensile strength of a material is the ratio of the maximum load that the material can withstand without fracture when it is being stretched, relative to the original cross-sectional area of the material. When the tension is less than the tensile force the material or part of it returns to its original shape. As the tensile values approach the values of the tensile force, the material tends to rupture (Fig. 3) [13].

The chemical degradation of the insulation makes wires more fragile, a phenomenon that we intend to detect with this test.

In this study, the tensile strength (Eq. (2)) and the elongation until breaking (amount of uniaxial deformation at the break point) were calculated (Eq. (3)).

$$S = \frac{F}{Ao} \tag{2}$$

$$\varepsilon = \frac{(lf - lo)}{lo} \tag{3}$$

3. Test Results

3.1 Characterization of Weld Formation

Capability study was done using 125 welded samples using wires of cross section 0.50 mm² and insulated with PVC and ETFE. Samples were created using three wires of same cross section and same type of insulation (Fig. 4). It was removed the wires on the top of the splice using a pull force measurement device and the force needed to remove or break the wire was registered. With the results a Ppk was calculated according to Figs. 5 and 6.

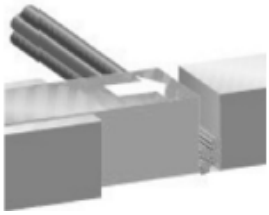

Fig. 4 Schematic of wire positioning on ultrasonic welding equipment.

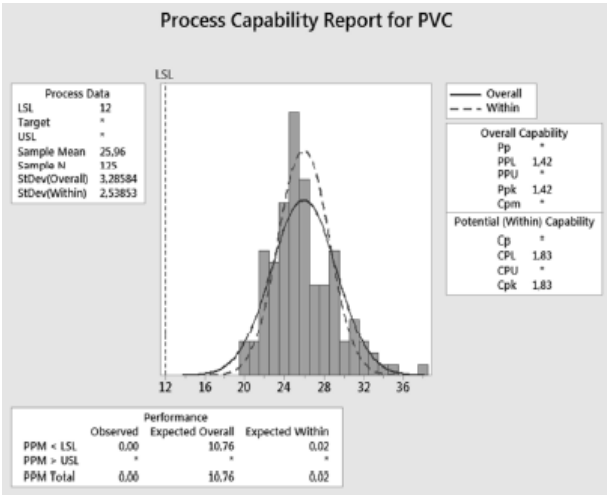

Fig. 5 Capability study for wires insulated with PVC.

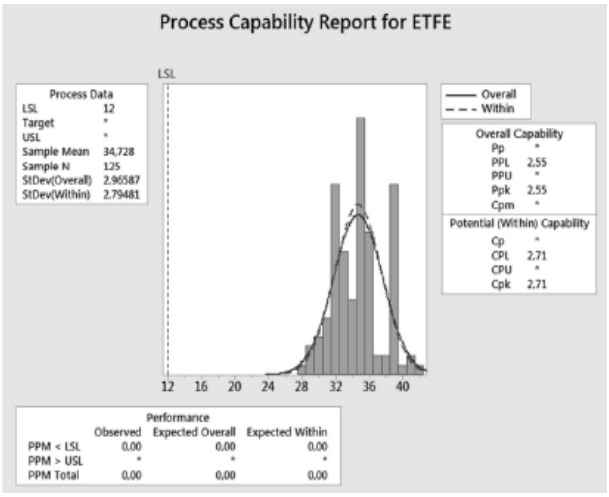

Fig. 6 Capability study for wires insulated with ETFE.

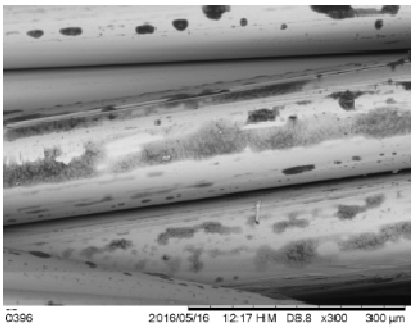

Fig. 7 PVC insulated wire analyzed by SEM.

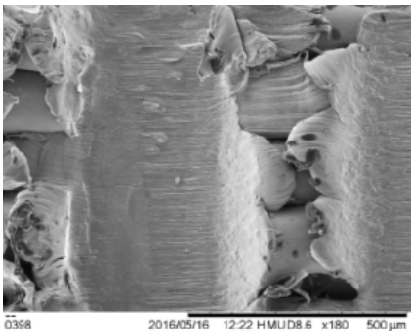

Fig. 8 Welded sample analyzed by SEM.

As results of Ppk for wires insulated with PVC were lower than expected, samples were analyzed on microscope to determine what may be causing the negative effect. Figs. 7 and 8 show the result of samples analyzed on SEM (Scanning Electron Microscope).

Samples showed some organic materials on the surface of copper strands that are causing the bad results as when samples were cleaning the results on Ppk were significantly increased.

Results of SEM analysis on ETFE insulated cables are shown in Fig. 9 and did not had any material on copper surface and the Ppk results were much higher than on wires insulated with PVC.

3.2 Analysis of Insulation Material when Submitted to Different Thermal Conditions

FTIR analysis was done to PVC to define if components are migrating to copper surface. Wire samples were tested at RT and heated at 40 ºC and 70 ºC (Fig. 10). It should be mentioned that working temperature for PVC wires is 105 ºC and for ETFE is 150 ºC.

For ETFE FTIR was also done even knowing no major issues were found (Fig. 11).

To determine the tensile strength (Table 1) and percentage of elongation of insulation materials (Table 2), samples were tested using a Zwick-Roell tensile test machine and Force versus Strain graphs were created (Figs. 12 and 13). Samples of PVC and ETFE were tested at RT and after heating at 40 ºC and 70 ºC.

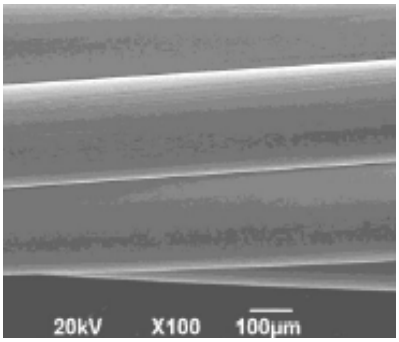

Fig. 9 SEM analysis of ETFE insulated wire.

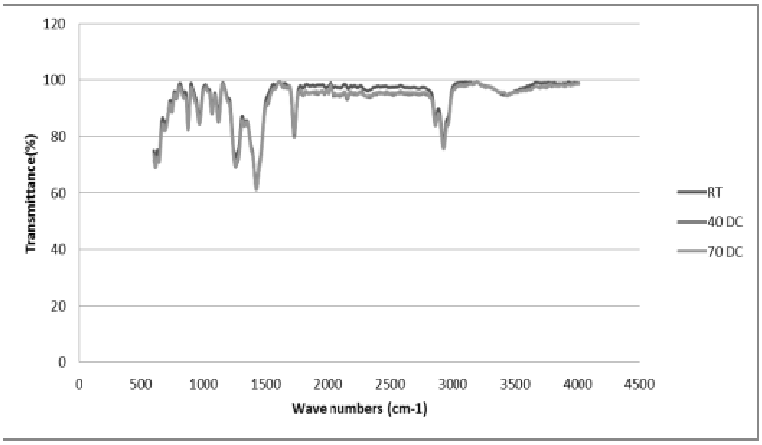

Fig. 10 FTIR for PVC insulation.

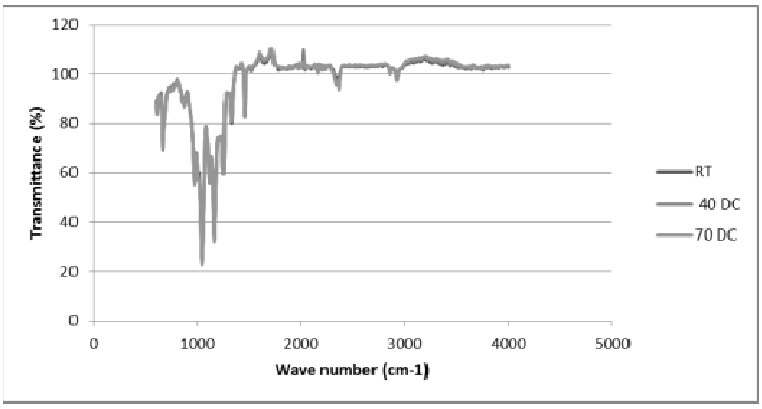

Fig. 11 FTIR for ETFE insulation.

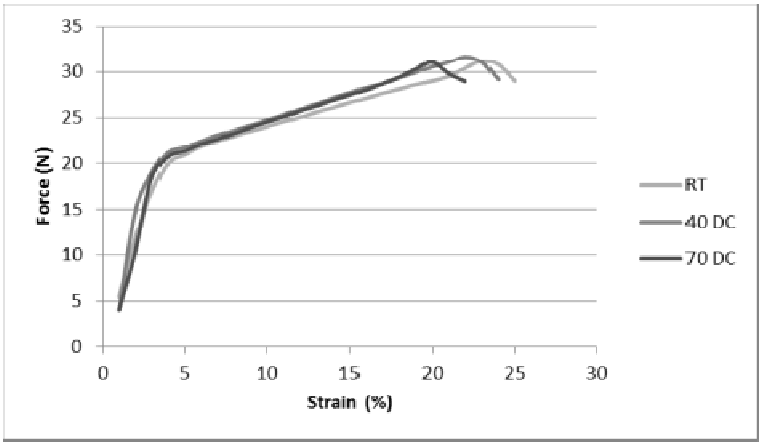

Fig. 12 Strength test for PVC.

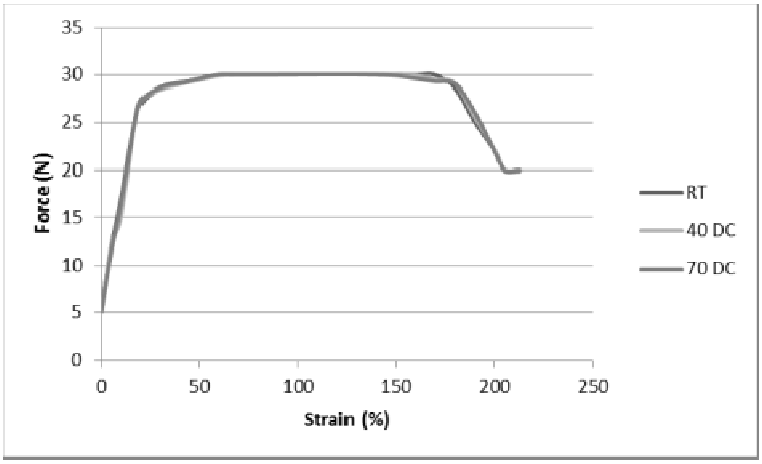

Fig. 13 Strength test for ETFE.

Table 1 Tensile strength for PVC and ETFE.

Tensile strength (N/mm²)						
Insulation material	PVC			ETFE		
Temperature (°C)	RT	40	70	RT	40	70
Force (N)	31.10	31.20	32.00	27.50	27.30	27.10
Area (mm²)	2.01	2.01	2.01	1.96	1.96	1.96
Tensile strength (N/mm²)	15.47	15.52	15.92	14.03	13.93	13.83

Table 2 Tensile strength for PVC and ETFE.

Elongation (%)						
Insulation material	PVC			ETFE		
Temperature (°C)	RT	40	70	RT	40	70
Sample length (mm)	50.00	50.00	50.00	50.00	50.00	50.00
Length till break (mm)	107.50	112.00	110.00	129.74	132.40	132.30
Enlongation (%)	115.00	124.00	120.00	159.48	164.80	164.60

4. Conclusions

On PVC infrared spectrum the vibrational stretches of the C-Cl bond appears in the range of 700-600 cm^{-1}, have a complex origin and depend on the conformational structure of the polymer and the arrangement of the atoms near the C-Cl bond. The remaining bands in the spectrum correspond to different vibrations of C-C and C-H. In PVC, the C-H bond stretch of HCCl may be considered as major bands at 2,970 cm^{-1}, stretching the CH bond of the CH_2 at 2,912 cm^{-1}, deformation of the CH_2 at 1,435 and 1,427 cm^{-1}, deformation of the CH bond of the HCCl at 1,331 and 1,255 cm^{-1}, at 1,099 cm^{-1} and the rotation of the CH_2 bond at 966 cm^{-1} [14]. On this infrared spectrum it was possible to identify the characteristic of PVC bands as well as the bands referring to the different vibrations of the C-C and C-H bonds. The spectrum of material submitted to different temperatures did not show variation, which is the reason why it is concluded that the temperature does not affect the structure of the PVC.

The ETFE infrared spectrums are characterized by the existence of vibrational stretching of the CF bond between 1,365-1,120 cm^{-1}, by a small vibration band of the CH bond between 3,125 and 3,040 cm^{-1} and by a band of varying intensity for the C=C between 1,680 and 1,620 cm^{-1}. The characteristic strain bands can be found between 1,000 and 905 cm^{-1}, at about 890 cm^{-1}, between 730 and 665 cm^{-1} and between 1,820 and 1,785 cm^{-1} [14]. In the spectrum obtained, it was possible to identify the main characteristic bands for ETFE and it was possible to conclude that ETFE, under the test conditions, did not change its structure.

Considering the tests done on tensile strength it was observed that insulation materials were not affected by the temperature variation. However, when analyzing the core of the wires it was seen on the surface of copper some pollutants, mainly carbon and oxygen that were initially supposed that they may be due to migration of insulation components to copper surface but after deep analysis, it was seen that compositions of polluted areas were different from compositions of insulation material. Based on that, it was concluded that the copper may be polluted before extrusion process. It was not possible to confirm the condition of copper before extrusion but it was proposed to be analyzed in a future work.

References

[1] https://ewi.org/the-advancement-of-ultrasonic-metal-welding-tool-materials/.

[2] http://www.thefabricator.com/article/arcwelding/understanding-ultrasonic-welding.

[3] Vries, E. 2004. "Mechanics and Mechanisms of Ultrasonic Metal Welding." The Ohio State University.

[4] Flood, G. 1997. "Ultrasonic Energy Welds Copper to Aluminum." *Welding Journal* 76 (1): 43-5.

[5] Zhang, C., and Li, L. 2009. "A Coupled Thermal-Mechanical Analysis of Ultrasonic Bonding Mechanism." *Metallurgical and Materials Transactions B* 40: 196-207.

[6] Lee, D. K., Kannatey-Asibu Jr, E., and Cai, W. 2012 "Ultrasonic Welding Simulations for Multiple, Thin and Dissimilar Metals." Presented at ASME International Symposium on Flexible Automation, St. Louis.

[7] Annoni, M., and Carboni, M. 2011. "Ultrasonic Metal Welding of AA 6022-T4 Lap Joints: Part I—Technological Characterization and Static Mechanical Behavior." *Science and Technology of Welding & Joining* 16: 107-15.

[8] Nică, L., and Gubencu, D. 2014. "Quality Analysis of the Ultrasonic Welding Process of Automotive Electric Wires, Nonconventional Technologies Review." Romania.

[9] www. schunk-sonosystems.com.

[10] LV112. 2007. *Electrical Cables for Motor Vehicles, Single-Core, Un-shielded*. Revision Date 16.01.

[11] Atkins, P. W. 1994. *Physical Chemistry* (5th Edition). Oxford: Oxford University Press, p. 543.

[12] DIN EN 60811-1-1. *Common Test Methods for Insulating and Sheathing Materials of Electric Cables and Optical Cables*. Methods for General Application-Tests for Determining the Mechanical Properties.

[13] Gendey, R. 2017. "Measurement Errors in Mechanical Testing." *Advanced and Material Processes Magazine—Automotive Materials* 165 (4): 2.

[14] Gunzeler, H., and Gremlich, H. 2002. *IR Spectroscopy: An Introduction*. Weinheim: Whiley-VCH, pp. 171-253.

Journal of Environmental Science and Engineering A 7 (2018) 132-139
doi:10.17265/2162-5298/2018.03.004

Main Steps for Radiopharmaceuticals Hot Cells Validation in Accordance with GMP Requirements: Methodology and Practical Guide

Fábio Eduardo de Campos[1], Efrain Araujo Perini[1], Carlos Leonel Zapparoli Júnior[1], Wilson Aparecido Parejo Calvo[1] and Valeriia Niowaveinc Starovoitova[2]

1. Nuclear and Energy Research Institute (IPEN), the University of São Paulo, São Paulo, SP 05508-000, Brazil

2. NiowaveInc, 1012 N Walnut St, Lansing, MI 48906, USA

Abstract: The worldwide GMP (Good Manufacturing Practices) guidelines issued for injectable pharmaceuticals globally agree that the vials filling operation must be performed under air cleanliness Grade A. The air cleanliness classifications adopted by the WHO (World Health Organization) define the particle diameter size, the sampling occupancy state and the limit concentration of viable particles. To reach conformity regarding the microbial limits foreseen at the GMP guidelines, a microbiological monitoring program must be stablished for selected sampling points such as active air sampling, passive air sampling (settle plate method), surfaces sampling (contact method), personnel sampling (gloves and clothes), compressed gas, materials and equipment that may interfere and compromise the product microbiological quality. The key elements for a GMP certification are directly related to a qualification and validation program for radiopharmaceutical manufacturers that must be clearly defined and documented by a validation master plan, foreseen by the manufactures Quality Assurance office. This study describes each qualification step and test for DQ (Design Qualification), IQ (Installation Qualification), OQ (Operation Qualification) and PQ (Performance Qualification) that must be carried out and carefully planned when it comes to hot cells and isolator systems in accordance with the GMP requirements foreseen by international regulatory and supervisory bodies.

Key words: Injectable radiopharmaceuticals, GMP, qualifications, regulations.

1. Introduction

Radiopharmaceuticals are known as injectable radioactive pharmaceuticals widely used for internal radiotherapy for cancer and diagnostic imaging for several body-malfunctions and its usage and applications can be found elsewhere, specially into the nuclear medicine field [1-4]. One must be aware that each country national's health surveillance regulatory authority must approve radiopharmaceuticals, before they can be commercialized and used in humans being.

When analyzing injectable pharmaceuticals production environments one must be aware the product may or may not represent contamination risks to the operator. It is not rare the situations in which it is not enough to protect the product against potential contamination from the environment, but the operator must be protected against being contaminated by handling product. In these cases, isolators represent important roles for the production environment. Isolators can be used to avoid such contaminations, its effectiveness must be reliable and several tests are carried on in order to validate its efficacy. It is worth to mention the air tightness test (carried out accordingly to ISO 10648-2) [5], which is one of the most important acceptance tests. Other tests that can be mentioned for the PQ (Performance Qualification) tests and still applied during the periodic qualification process are HEPA (High Efficiency Particulate Air) filters leakage test, air flow, air changes, air velocity

Corresponding author: Fábio Eduardo de Campos, master, research field: nuclear technology and applications in radiopharmacy facilities.

and unidirectional flow uniformity test, lighting intensity test, particle counting test (at rest and during operation states) and, finally, it is necessary to assure operational condition under negative pressure gradient [6].

For a reliable environment, the radiopharmaceutical production must be focused on the operator safety and product protection, this present work alerts the responsibility for hot cells buyers and manufacturers, and also for the current in-use hot cells regarding its technical aspects and operational conditions, especially the current ones, which are already radioactively contaminated and may present potential risks to the environment and to the operator if some of the qualification test parameters are not taken into consideration. Therefore, more than knowing which the requirements for the production environment are, it is better to know how to reach and meet each of them and mainly, how to maintain them into the requirement levels and tolerances foreseen by the guidelines and reference regulations bodies, such as, the FDA (Food and Drug Administration) [7], the rules governing medicinal products in the European Union (EudraLex) [8], the International Pharmacopoeia (issued by the WHO (World Health Organization)) [9] and others.

2. Isolators and Hot Cells Requirements

Isolators concepts and philosophies are similar to a microenvironment design and its applications to laboratories can be found elsewhere [10]. It can be used not only for protecting the product against contamination, but also for protecting the operator against toxic compounds or for both protections (product and operator) simultaneously. Hence the sealed microenvironment idea is to ensure high levels for viable and non-viable particles controlling into it yielding a reliable and aseptic manufacturing process while it also protects the external environment and the operator.

The utilization of isolator technology minimizes human intervention in processing areas and may result in a significant decrease in the risk of microbiological contamination of aseptic manufactured products from the environment. There are many possible designs of isolators and transfer devices. The isolator and the surrounding environment should be designed so that the required air quality for the respective zones can be achieved. Isolators are constructed using puncture resistant materials and preventing air leakage. Transfer devices may vary from a single door to double door designs and fully sealed systems incorporating sterilization equipment. The transfer of processing materials into and out of the unit is one of the greatest potential sources of contamination. In general the area inside the isolator is the zone for high risk manipulations, although it is recognized that unidirectional air flow may not exist in the working area of all such devices. The air classification required for the background environment depends on the design of the isolator and its application. It should be controlled and for aseptic processing it should be at least grade D. Isolators should be introduced only after appropriate validation. Validation should take into account all critical factors of isolator technology, for example the quality of the air inside and outside (background) the isolator, sanitization of the isolator, the transfer process and isolator integrity. Monitoring should be carried out routinely and include frequent leak testing of the isolator and glove/sleeve system.

Therefore a hot cell can be understood as an isolator, though it has special design and assembling techniques in order to provide its correct usage such as an ergonomic operation and the radiation shielding. Also the material handling inside a hot cell (or containment enclosure) requires an “hourly leak rate” which is related to the processing material dangerousness and, consequently, the hot cell or the “containment” classification can be categorized into four classes, as shown in Table 1.

It is worth to mention that the leak test is carried out at FAT (Factory Acceptance Test) or SAT (Site Acceptance Test) steps and if the isolator or hot cell

Table 1 Classification of containment enclosures accordingto their hourly lake rate (adopted from ISO 10648-2 [5]).

Class	Hourly lake rate ($Tf \cdot h^{-1}$)	Example
*1	$\leq 5 \times 10^{-4}$	Containment enclosure with controlled atmosphere under insert gas conditions
*2	$< 2.5 \times 10^{-3}$	Containment enclosure with controlled atmosphere under inert gas conditions or with permanently hazardous atmosphere
3	$< 10^{-2}$	Containment enclosure with permanently hazardous atmosphere
4	$< 10^{-1}$	Containment enclosure with atmosphere which could be hazardous

*The classification of leak tightness required for a particular application under classes 1 and 2 shall be decided by the designer and licensing authorities. Normally, class 1 will be applied for technical reasons when higher gas purity is required.

fails in this test the manufacturer must review the isolator structure, cracks and sealing.

Accordingly to ISO 10648-2, the leak test for isolators can be performed by the pressure change method, which takes into account corrections due to variations and atmospheric pressure. For acceptance test, the starting negative pressure should be four times greater than the working pressure condition. The leak tightness of containment enclosure must comply with the rate of leakage of a class 2 containment enclosure, in accordance with ISO 10648-2 [5] ($Tf < 2.5 \times 10^{-3}$ or < 0.25%).

Once the hot cell enclosure tightness requirement is achieved, the operation requirements now must be fulfilled in terms of negative pressure gradient. The standardization [6] states that for the handling of radioactive or toxic products, the enclosure is required to be at a negative pressure in relation to the room. This under pressure, the only one of such values easily monitored, is expressed in Pascal (Pa) or Decapascal (daPa), and generally ranges from 20 daPa to 50 daPa below room pressure. Its measurement enables a hierarchy of pressure to be maintained when different enclosures are connected.

3. Product Requirements

As a requirement for aseptic products manufacturing, the clean room in which operations are conducted has its air cleanliness according to the criticality of the environment. Each manufacturing process requires an appropriate environmental "in operation" condition to minimize the microbiological contamination risk, and other potential contamination such as product particles or particles from another used materials. It is interesting to highlight when considering "in operation" test for injectable radiopharmaceutical production hot cells. First of all, the fact that a hot cell does not allow the presence of the operator inside clearly avoids the primary contamination source, indeed GMP (Good Manufacturing Practices) requirements [11] shows that between 30,000 and 40,000 of human-being skin cells fall off every hour. Furthermore to keep the particle counting levels as required is not an easy task if the hot cell is not well designed; this task is related not only to the hot cell design aspects but also to the devices placed into it for the production processes such as crimpers, decrimpers, door opening and closing systems, and so many other devices required for a GMP certified production.

Some short half-life radiopharmaceuticals are usually injected to patients right after the manufacturing process and for this reason the quality control approving tests results are eventually post administrative, such as, sterility test, radionuclide purity test and others to its release and even to its injection. Then, the establishment of regulations and specifications to ensure a reliable radiopharmaceutical production is extremely required, especially for the "in operation" condition that is worldwide foreseen in the EudraLex GMP guidelines [12], such as:

- Grade A is equivalent to ISO class 4.8 "at rest" and to ISO class 5 "in operation". Grade A is equivalent to ISO class 5 for particles diameter size ≥ 0.5 μm (until 3,520 particles per m^3). However, when counting particles diameter size ≥ 5.0 μm Grade A is

equivalent to ISO class 4.8 once it tolerates maximum of 20 particles while ISO class 5 tolerates maximum of 29 particles. Thus Grade A is called ISO class 5 "in operation" for particles size ≥ 0.5 μm and ISO class 4.8 "at rest" for particles size ≥ 5.0 μm. Still regarding Grade A, the GMP guidelines stablish it as a "high operational risk zone for filling and aseptic connections. Normally those operations must be carried out under unidirectional flow conditions" [12];

- Grade B is equivalent to ISO class 5 "at rest" and to ISO class 7 "in operation" states for both particle diameter sizes. The GMP guidelines stablish that grade B is applied to "grade A surrounding area for preparations and aseptic fillings" [12];
- Grade C is equivalent to ISO class 7 "at rest" and to ISO class 8 "in operation" states for both particle diameter sizes;
- For grade D it is only defined the number of particles "at rest" state condition and together with the grade C, they are referred to clean areas where less critical processes are carried out for sterile products manufacturing.
- For a better understanding the EudraLex [12] brings Table 2 for the particle size and air cleanliness classification grades.

In order to face all the GMP requirements to the product and to the manufacturing environmental acceptance, it is required a PQ protocol to be stablished. It is important to mention the qualification process has its basis on the GMP guidelines and it must be developed based on its EudraLex [12].

The qualification process consists of several tests which are divided into small groups for a better task management and sequencing. Each qualification test must be associated to a test protocol where the test procedures and the acceptance criteria are pre-defined. The protocols must be filled out with each test result and the results must be confronted to the test acceptance criteria. After filling out the test protocol with the results the responsible for the test execution must sign the report. A representative counterpart (the hot cell buyer) also must sign the report confirming the tests methodology and results. During the test execution the reference documents must be available for verifications. The qualification can only be concluded when all the protocols are filled out and all the results are in accordance with the acceptance criteria stablished at the protocol.

4. Qualification Tests and Acceptance Criteria

When a radiopharmaceutical manufacturer starts a hot cell specification design, such as by developing the hot cell's URS (User Requirement Specifications), one must be aware of each step and responsibilities are undertaken within this hot cell purchasing process until its conclusion, which means, until the hot cell is qualified according to the GMP requirements. Fig. 1 brings a box-diagram that better illustrates this URS, design and qualifications steps.

When it comes to the hot cell qualification tests, either the hot cell manufacturer or the buyer must be aware of each test requirement to meet all the safety standards regarding to the operator protection and to the product protection, once an injectable radiopharmaceutical is being handled inside it. The

Table 2 The maximum allowed airbome particle concentration for each grade.

	Maximum permitted number of particles per m^3 equal to or greater than the tabulated size			
	At rest		In operation	
Grade	0.5 μm	5.0 μm	0.5 μm	5.0 μm
A	3,520	20	3,520	20
B	3,520	29	352,000	2,900
C	352,000	2,900	3,520,000	29,000
D	3,520,000	29,000	Not defined	Not defined

Source: adopted from EudraLex [12].

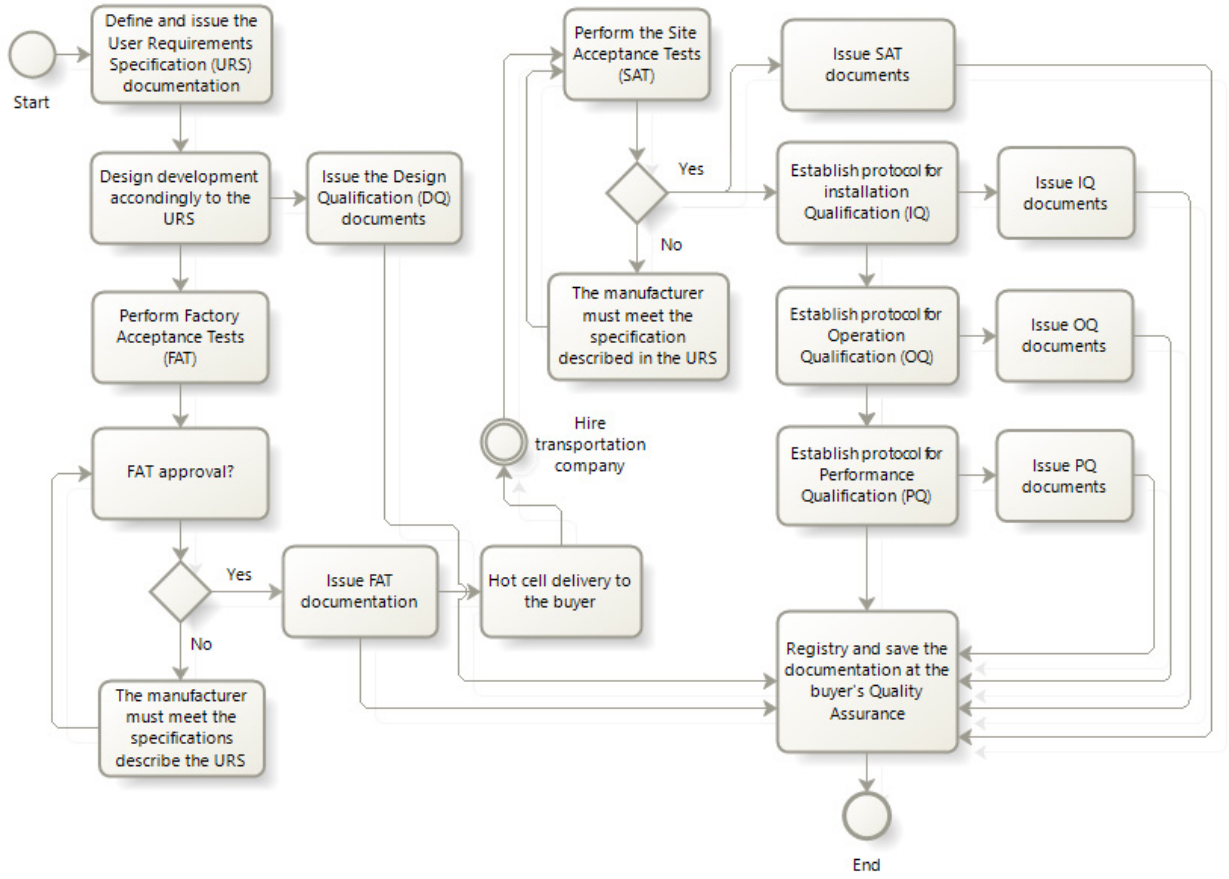

Fig. 1 Box-diagram for hot cell design, purchase and respective qualifications.

following tests are proposed in order to fulfill the hot cell qualification criteria for radiopharmaceuticals production. Each of the following tests has its protocol and the respective standardization reference, stablished as criterion.

4.1 Verification of Filter Integrity (Filter Leakage) for General HEPA Filter and for Unidirectional Flow Units

It is worth to highlight that hot cells require a high efficiency filtering system, either in the air intake (to guarantee the air quality into the hot cell), or in the air outflow (to avoid environmental radiologic contamination). As established by the standard ISO 14644-3 [13], this test is carried out to confirm if the final filtering system with high efficiency filters is properly installed and sealed to prevent leakage or possible contamination to the working area.

Goal: to ensure the HEPA filtering system is in accordance with the specifications regarding to filter integrity and tightness and also guarantee that this filter system fulfills the user requirements. This test does not verify the filtering system efficiency.

Precondition: for traceability reasons, each installed HEPA filter must be supplied with the manufacturer's integrity test certificate and it must be attached to the qualification report.

Standards references:

- IEST-RP-CC006.2—Institute of Environmental Sciences and Technology [14];
- ISO 14644-3:2005—Clean rooms and associated controlled environments—Part 3: Test methods [13];
- ISO 15767:2009—Unidirectional flow clean-air devices—Requirements and test methods [15].

Acceptance criteria:

The filters can be tested following the uranine test

or the DOP (Dispersed Oil Particulate) test. The uranine test has efficiency of 99.98% (the uranine particles dimension is 0.15-0.18 μm); while the DOP test has efficiency of 99.993% (the DOP particles dimension is 0.3 μm). Despite the minor difference in both efficiencies (the DOP test efficiency is higher because the DOP particles are bigger) the filter efficiency remains the same for both tests:

- The upstream aerosol concentration must lay between 20-100 μg/L and the filter leakage level must be ≤ 0.01% of the upstream;
- Filter repair limits—total repair area must be ≤ 3% of the face area of the filter and the smallest dimension of any repair must be ≤ 3.8 cm;
- Filter pressure drop—defined by the manufacturer (measured in Pa).

4.2 Verification Filter One-Way Flow Speed (with Unidirectional Flow Only)

Goal: to check the filter downstream air velocity.

Precondition: the filter integrity test must be done and approved according to the test acceptance conditions.

Standards references:

- ISO 15767:2009—Unidirectional flow clean-air devices—Requirements and test methods [15].

Acceptance criteria:

- The downstream air velocity must be within 0.36 m/s and 0.54 m/s;
- The air flow uniformity velocity deviation must be ≤ 15 %.

4.3 Air Change or Air Change Rate Verification

Goal: to check the air change inside a chamber, room or any controlled environment.

Precondition: all equipment must be operating.

Standards references:

- AABC (Associated Air Balance Council)—Test & Balance Procedures [16];
- ANSI/ASHRAE 111-2008 (RA 2017)—Measurement, Testing, Adjusting and Balancing of Building HVAC Systems [17];
- AMCA 203-90—Air Movement and Control Association International, Inc. [18];
- ISO 14644-3:2005—Clean rooms and associated controlled environments—Part 3: Test methods [13];
- ISO 15767:2009—Unidirectional flow clean-air devices—Requirements and test methods [15].

Acceptance criteria:

(a) The air change rate must be ≥ 20 air changes per hour (20 ac/h).

4.4 Lighting Intensity Verification

It is worth to highlight that, although this verification test is not mandatory, it should be considered during the (factory) acceptance tests because the lighting operating conditions of a hot cell have at least two constraints to consider. First, the hot cells operators need to handle the materials using tele-pliers and check the inner operations through lead glasses windows, which limit the vision by its density and color. Second, it must be considered that minimal lighting intensity may vary from each operator, once visual condition is physiological and it is related to each person.

When searching about lighting intensity guidelines for hot cells, there is no specific study for hot cells, except for one IAEA Safety Series publication [19]. It must be considered this publication is dated from 1981 and the search for an updated study is still required. Thus the only reference we could use is the guidelines [20], which adopts 500 lux for pharmaceutical productions, although it does not consider the lead glass windows, used in the hot cells. Therefore, if one considers the standard adopted by the hot cells manufactures as “around 1,000 lux on the work surface”, it seems to be very reasonable.

4.5 Non-viable Particles Counts Verifications (at Rest)

Goal: to ensure the non-viable airborne particle concentration of 0.5 μm and 5.0 μm of the tested environment at “at-rest” occupancy state is below the

allowable particle concentration according to the designed ISO class.

Precondition: the clean room or controlled environment must be previously cleaned. The test must be performed with the ventilation system in operation. All the internal equipment (filling systems, crimpers, etc.) must be turned on and neither tele-pliers nor tongs should be maneuvered.

Standards references:

- ISO 14644-1:2015—Clean rooms and associated controlled environments—Part 1: Classification of air cleanliness by particle concentration [21];
- ISO 14644-3:2005—Clean rooms and associated controlled environments—Part 3: Test methods [13];
- Guidance PET drug products to Good Manufacturing Practices (CGMP-Annex 1) [22].

Acceptance criteria (at rest), based on the FDA [22]:

As shown in Table 1 for particle concentrations and average size:

- Grade A (ISO class 4.8 air cleanliness classification) at one single air sampling location;
- Grade B (ISO class 5 air cleanliness classification) at one single air sampling location;
- Grade C (ISO class 7 air cleanliness classification) at one single air sampling location;
- Grade D (ISO class 8 air cleanliness classification) at one single air sampling location.

4.6 Non-viable Particles Count Verifications (in Operation)

Goal: to ensure the non-viable airborne particle concentration of 0.5 μm and 5.0 μm of the tested environment at "in-operation" occupancy state is below the allowable particle concentration according to the designed ISO class.

Precondition: for this particular verification test applied to hot cells, the "in operation" state will be called as "in-dynamical-operation" state because when it comes to an isolator chamber, the tested environment does not have the presence of the operator inside it. Thus the procedure is to simulate, with non-radioactive materials (using water), all the manufacturing process "in-dynamical-operation", such as pass-through doors opening, internal devices operations (vials crimpers, decrimpers, vials fractionating and filling systems, ionization chambers), materials outtake, waste disposal etc., so those operations will indicate if the tested hot cell can fulfill the requirements for the dynamical-operational state.

Guidelines references:

- ISO 14644-1:2015—Clean rooms and associated controlled environments—Part 1: Classification of air cleanliness by particle concentration [21];
- ISO 14644-3:2005—Clean rooms and associated controlled environments—Part 3: Test methods [13];
- Guidance PET drug products to Good Manufacturing Practices (CGMP-Annex 1) [22].

Acceptance criteria (in operation), based on the FDA [22]:

(a) The same criteria are used for the non-viable particles counts verifications (at rest).

5. Conclusions

A detailed and critical URS for a new hot cell is the bottom line to a successful validation process to comply with GMP requirements.

One must be aware of each design and manufacturing step of an isolator-like equipment or hot cell, starting at the DQ (Design Qualification), then the upcoming FAT (Factory Acceptance Test), after the equipment delivery and installations the buyer must require the SAT (Site Acceptance Test), then the IQ (Installation Qualification), the OQ (Operational Qualification), and the PQ. The analyses of the results obtained during the PQ tests and the evaluation of the conformities (and non-conformities) are the last step for the complete equipment acceptance, which must be under the responsibility of the manufacturer, but also under the buyer Quality Assurance.

Finally, it is worth to mention that the buyer must be aware about the validation and acceptance tests

methodology and instrumentation, once the manufactures may hide some features or criteria in order to show the tested equipment completely approved by the "company" tests, and sometimes the "company tests" has not the same criteria as the GMP requirements and criteria to ensure safety and security to operators, surrounding environment and finally to the patient who will be injected with the radiopharmaceutical produced in these isolators and hot cells.

This study shows the relevance of the primary steps toward successful acceptance criteria aiming the GMP qualification of hot cells and isolators. It also brings international references standards and guidelines to support information to users and manufactures along with orientations toward acceptance and qualification tests. The next studies on radiopharmaceuticals hot cells certification in accordance with GMP requirements will bring practical qualification tests results and discussions (set up guide), and the final study will conclude with a microbiology growth comparison according to the hot cell internal chamber stainless steel surface finishing.

References

[1] Krebs, S., and Dunphy, M. 2017. "Chapter 17: Role of Nuclear Medicine in Diagnosis and Management of Hepatopancreatobiliary Disease." *Blumgart's Surg Liver, Biliary Tract Pancreas* 2: 285-315. doi: 10.1016/B978-0-323-34062-5.00017-0.

[2] Abram, U., and Alberto, R. 2006. "Technetium and Rhenium—Coordination Chemistry and Nuclear Medical Applications." *J. Braz. Chem. Soc.* 17: 1486-500. doi: 10.1590/S0103-50532006000800004.

[3] Sharp, P. F., and Gemmell, H. G. 2005. *Practical Nuclear Medicine*. Springer.

[4] Schmor, P. W. 2010. "Review of Cyclotrons Used in the Production of Radioisotopes for Biomedical Applications." In *Proc. CYCLOTRONS 4:420*. doi: http://dx.doi.org/10.1142/S1793626811000574.

[5] International Organization for Standardization (ISO). 1994. Classification according to Leak Tightness and Associated Checking Methods (ISO 10648-2).

[6] International Organization for Standardization (ISO). 2001. "Part 4: Ventilation and Gas-Cleaning Systems such as Filters, Traps, Safety and Regulation Valves, Control and Protection Devices (ISO 11933-4)." In *Components for Containment Enclosures*.

[7] U.S. Food & Drug Administration. https://www.fda.gov/.

[8] EudraLex—EU Legislation. https://ec.europa.eu/health/documents/eudralex_en.

[9] World Health Organization (WHO). 2017. *The International Pharmacopoeia* (7th ed.) http://apps.who.int/phint/en/p/about/.

[10] ASHRAE. 2015. "ASHRAE Laboratory Design Guide: Planning and Operation of Laboratory Hvac Systems."

[11] Chaloner-Larsson, G., and Anderson, R. E. A. 1997. "Part 2: Validation. World Heal Organ 100." In *A WHO Guide to Good Manufacturing Practice (GMP) Requirements.*

[12] European Commission. 2008. EudraLex—The Rules Governing Medicinal Products in the European Union. V.4. EU Guidelines to Good Manufacturing Practice Medicinal Products for Human and Veterinary Use. Annex 1. Manufacture of Sterile Medicinal Products.

[13] International Organization for Standardization-ISO. 2005. "Part 3: Test methods (ISO 14644-3:2005)." In *Cleanrooms and Associated Controlled Environments*.

[14] Institute of Environmental Sciences and Technology-IEST. 2004. Testing Cleanrooms (CC006.2).

[15] International Organization for Standardization-ISO. 2009. Unidirectional Flow Clean—Air Devices: Requirements and Test Methods (ISO 15767:2009).

[16] Associated Air Balance CounciL (AABC). 2002. *National Standards for Total System Balance*, USA.

[17] American National Standards Institute (ANSI), American Society of Heating, Refrigerating and Air-conditioning Engineers (ASHRAE). 2008. Measurement, Testing, Adjusting and Balancing of Building HVAC Systems (ANSI/ASHRAE-111-2008, RA 2017).

[18] Air Movement and Control Association Iinternational I-A. 2011. Field Performance Measurement of Fan Systems (AMCA 203-90, R 2011).

[19] International Atomic Energy Agency (IAEA). 1981. *Manual on Safety Aspects of the Design and Equipment of Hot Laboratories*. Procedures and Data (Safety Series No. 30), Vienna.

[20] Association Française de Normalisation-AFNOR. 2011. "Part 1: Indoor Work Places (NF EN 12464-1)." In *Light and Lighting—Lighting of Work Places*.

[21] International Organization for Standardization-ISO. 2015. "Part 1: Classification of air cleanliness by particle concentration (ISO 14644-1)." In *Cleanrooms and Associated Controlled Environments*.

[22] U.S. Food and Drug Administration (FDA). 2005. *Guidance PET Drug Products—Current Good Manufacturing Practice (CGMP)*. Draft Guidance.

Journal of Environmental Science and Engineering A 7 (2018) 140-145
doi:10.17265/2162-5298/2018.03.005

Valuation of the External Cost Caused by the Environmental Pollution of Three Lakes in Northern Greece

Odysseas Kopsidas

Department of Industrial Management and Technology, University of Piraeus, Piraeus 18534, Greece

Abstract: The preservation/restoration of natural environment is usually entailing high cost mostly paid by citizens through taxes. The effect of these taxes is double. The direct effect is the obvious additional income for the State, and the indirect effect is an additional income for the citizen, due to increasing tourism. Since the evaluation of this good cannot be in market terms, authors apply a modified CVM (Contingent Valuation Method), which is part of Experimental Economics, in order to find out the order of concern that people have about natural environment. Authors also, try to investigate their WTP (Willingness To Pay) for supporting activities for preservation/restoration of three lakes in Northern Greece, in particular, lake of Ioannina, lake of Florina and lake of Kastoria. For the purpose of this research, authors use parametric and non-parametric approaches, as well as Linear Regression and Logic Models.

Keywords: Valuation method, CVM, natural environment, WTP, Logit Model, linear regression, parametric and non-parametric approaches.

1. Introduction

Wetlands—and especially lakes—are the most productive ecosystems in the world. They support plenty of ecological activities and important natural habitats. These ecological activities translate strictly into economic functions and services such as flood protection, water supply, improved water quality, commercial and recreational fishing and hunting [1]. Although, it is a common knowledge that the multiple role of wetlands is usually biased towards the economics benefit from commercial use and exploitation. Usually, the natural benefits of wetlands are underestimated and the order of exploitation is so high that leads to the extensive degradation [2]. Despite the uncertainty in total area of wetlands around the world, there are some figures indicating the importance of the problem. In Europe, 50% to 60% of wetlands have been lost in past century due to the human intervention, while the United States has lost 54% of its original wetlands [3]. The accelerated rate of wetlands loss was a great alarm for many countries and scientists around the world to take care of the situation. In 1971, more than 100 countries created the Ramsar Convention of Wetlands of International Importance, providing the first step for a greater international cooperation about the protection and the "wise use" of wetlands and their resources [4]. A increasing number of valuation studies on environmental sector contribute evidence about the importance of wetlands. Literatures provide a variety of studies which include many valuation methods, such as CVM (Contingent Valuation Method), replacement value method etc. [3], use 39 wetlands valuation studies to create a meta-analysis using CV method [4], also created a meta-analysis of 30 Contingent Valuation applications. A few years later [5], made a meta-analysis using 190 wetlands valuation studies [6].

Despite the fact that there is a great international scientific concern about the restoration and protection

Corresponding author: Odysseas Kopsidas, Ph.D., research fields: public and environmentlal economics.

of wetlands, in Greece, there are only a few studies. In literature, it is used CVM to evaluate stakeholders' preferences among four possible hypothetical scenarios for a wetland in Lesvos Island [7, 8]. Another CV research estimates the use values of ecological functions of Zazari-Cheimadidita wetland. In present study, authors are using CVM to valuate three wetlands in Greece. In particular, authors are investigating the WTP (Willingness To Pay) of local citizens to preservation/restoration of three lakes in Northern Greece, lake of Ioannina (lake Pamvotida), lake of Kastoria (lake Orestiada) and lake of Florina (lake Cheimaditida). This research is organized in five sections. The first section is the introduction and previous relative works. In Section 2, authos present some information about each lake, which leads us to this research. In Section 3, authors present the data and the empirical analysis of the research. Last but not least, in Section 4 there are the conclusions, while the bibliography takes place in Section 5.

2. Knowing the Lakes

2.1 Lake of Florina (Lake Cheimaditida)

Cheimaditida is a lake of northern Greece, located 40 km south of the prefecture of Florina. It is one of the lakes formed among the mountains of Verno, Voras, Askio and Vermio. Among these mountains there are some more wetlands, like Lake Vegoritida, Lake Zazari etc.. Cheimaditida's surface is around 10.8 square km, its maximum length is 6.3 km and it is located in an altitude of 593 m. Its average depth is 1 meter and the maximum is 2.5 m. The water quality of Lake Cheimaditida is affected by household waste of the adjacent nine communities. Apart from this pollution, the quality of lake water is affected by livestock waste animals which are breeding around. However, the critical pollution factor is the excessive use of fertilizers and pesticides in crops, which end up in lake through ground dismantling. The level of Lake Cheimaditida has been dramatically reduced in recent decades, mainly due to irrigation, with adverse effects on the flora and fauna of the area. The Greek Biotope-Wetlands Center investigated the concern of local citizens (farmers, fishermen and local authorities) about the problem. The results declared the willingness of the citizens to pay for the restoration of the lake.

2.2 Lake of Kastoria (Lake Orestiada)

Lake of Kastoria, Orestiada, is located in Western Macedonia in western part of Kastoria Prefecture, northeast, east and southeast of the town of Kastoria and between the mountains of Verno, Aschi, Korissos and Vigla. Orestiada's surface is around 28 square km and located in an altitude of 630 m. Orestiada's average depth is around 3.5 meters and the maximum depth is 9.5 meters. The coast length is about 31 km. The water of the lake comes mainly from streams. In the area, there are nine streams leading to the lake. The largest of these is the stream of Xiropotamos. In addition to streams, rain water and snowfall, Lake Orestiada is also fed by many lush springs. Orestiada is an urban lake with intense human activity over the last decades, due to the threat of ecological balance of the area which is polluted by urban waste water, sewage effluents, fertilizers and solid waste. In Orestiada, the eutrophication phenomenon is intense, with all its negative effects on the quality of its water. The water of the lake, as the ultimate recipient of all natural processes, as well as the human activities, is constantly receiving loads of nutrients and other components and, in particular, phosphorus charges. According to results of a study which took place in lake of Kastoria [5], when the lake freezes almost every year, there is a decrease in oxygen and in the summer an increase in pollution due to agricultural activities.

2.3 Lake of Ioannina (Lake Pamvotida)

Lake of Ioannina (Lake Pamvotida) is located in the north-western part of Greece at an altitude of 470 meters above the sea level and is perhaps one of the

rare cases, where a lake has been connected so much to the history and like of a city, Ioannina. The lake is 7.5 km long, 1.5-5 km wide, has average depth 4-5 meters, maximum depth 11 meters and surface around 22.8 square km. It is surrounded by the Mitsikeli and Tomaros mountains and it is formed by water of three main springs. The drainage of the water takes place through the Lapista ditch and flows from the river Kalamas. The pollution of the natural environment of Lake Pamvotida and mainly of the lake's water derives from human activities related to the city of Ioannina, small and large communities and residential areas located around, as well as the industrial output. The main source of pollution of the lake is urban and industrial waste water, as well as the waste of a large number of poultry farms, pig farms and cheese dairies in the area, many of which are illegal. Around 75% of the output of these farms is transferred indirectly to the lake resulting a crucial pollution to the water.

3. Data and Empirical Results

3.1 Data

In order to investigate the WTP of the citizens around each lake, authors took three random samples from each town (Ioannina, Florina and Kastoria) and authors asked them to complete some questionnaires. Authors took 60 questionnaires from citizens of Florina, 90 questionnaires from citizens of Ioannina and 80 questionnaires from citizens of Kastoria. The main question authors asked on each interviewee is the amount of money that he/she is willing to pay per month in order to restore the lake of his/her town. Authors also asked their opinion about the lake and their living distance from the lake. A list of variables which were tested is the following.

3.2 Empirical Results

In the first part of the analysis authors present some descriptive statistics about citizens' willing to pay in each town. In Table 1, it is the list of variables. In Table 2, it is presented the descriptive statistics for WTP.

On the one hand, descriptive statistics provide evidence that citizens of Kastoria are willing to pay more for the restoration of the lake. On the other hand, citizens of Ioannina are willing to pay far less for the restoration of their lake.

Table 1 List of variables.

X_1 :	Visiting the lake
X_2 :	Way of information about the lake condition
X_3 :	Ecological condition of the lake
X_4 :	Main problem of the lake
X_5 :	Reason of the ecological problem
X_6 :	Authorities' concern about the lake
X_7 :	Membership of an ecological organization
X_8 :	Local authorities participation every 100 euro
X_9 :	People participation every 100 euro
X_{10} :	What do you wish to be done?
X_{11} :	WTP for the restoration
X_{12} :	Willingness to pay for the restoration if you were living next to the lake (WTP1)
X_{13} :	What do you want to restore first?
X_{14} :	Amount of money that you would accept in order not to restore the lake Willingness to Pay (WTA)
X_{15} :	Industries
X_{16} :	Gender
X_{17} :	Age
X_{18} :	Living
X_{19} :	Heritage close to the lake
X_{20} :	Working around the lake

Table 1 to be continued

X_{21} :	Distance from the lake
X_{22} :	Working condition
X_{23} :	Work relative to the lake
X_{24} :	Marital status
X_{25} :	Members of the family
X_{26} :	Education level
X_{27} :	Income according to citizen in Northern Greece
X_{28} :	Income according to citizen of the town

Table 2 Descriptive statistic for WTP of the citizens of each town.

	Mean	Standard deviation	Range	Min	Max
Ioannina	1.99	0.772			
Kastoria	13.16	11.221	50		
Florina	8.22	12.356	50		

Table 3 Linear regression model for each lake.

Town	Linear Regression Model
Ioannina	$X_{11} = 0.195 * X_4 + 0.349 * X_6 - 0.174 * X_{10} - 0.595 * X_{12}$
Kastoria	$X_{11} = 1.164 - 0.279 * X_9 + 0.82 * X_{12} - 0.147 * X_{14} - 0.173 * X_{19} + 0.113 * X_{28}$
Florina	$X_{11} = 0.743 + 0.222 * X_7 - 0.322 * X_9 + 0.581 * X_{12} - 0.174 * X_{19}$

Table 4 ANOVA for every model of each town.

Town	Model	Sum of squares	Df	Mean square	*F* statistic	Sig
	Regression	36.408	19	1.916	19.851	
Kastoria	Residual	5.792	60	0.097		
	Total	42.200	79			
	Regression	39.670	25	1.587	7.625	
Ioannina	Residual	13.319	64	0.208		
	Total	52.989	89			
	Regression	39.421	19	2.075	4.762	
Florina	Residual	17.429	40	0.436		
	Total	56.850	59			

In the next part of the analysis, authors estimate a linear regression model with dependent variable $X1_1$ (WTP). One of the main supposes of linear regression is the absence of multi-collinearity between the independent variables. In order to examine the existence or absence of multi-collinearity authors estimate a VIF (Variance Inflation Factor) test in SPSS. From this test, authors observe that $X1_7$ and $X2_2$ have VIF-value higher than the other values. In order to solve this problem, authors choose to exclude $X1_7$ from the model. Then authors estimate the linear model with remain variables for each lake and the results can be observed in Table 3.

The coefficients which were not statistically significant are excluded from the models.

Coefficients were examined in 5% level of significance.

Table 3 provides evidence that only few variables can affect the WTP of the local citizens. Some variables were found statistical significant in every model and some variables only in one model. This happens because every area in Greece has its own particularities.

In the next step of the analysis, authors made a variance analysis (ANOVA) of each model, in order to examine if there is a good adaptation of the

Table 5 Logit model fitting information.

Town	Model	-2 Log Likelihood	Chi-square	Df	Sig
Kastoria	Intercept Only	175.04			
	Final	0.000	175.049	19	
Ioannina	Intercept Only	199.351			
	Final	76.177	123.174	24	
Florina	Intercept Only	152.153			
	Final	78.925	73.228	19	

Table 6 Logit estimation result.

Town	Variable affect WTP (sign)
Kastoria	$X_{12}(+), X_{13}(+), X_{14}(-), X_{19}(+)$
Ioannina	$X_{1}(-), X_{4}(+), X_{6}(+), X_{10}(-), X_{12}(+), X_{15}(+)$
Florina	$X_{10}(-), X_{12}(+), X_{24}(-)$

theoretical model. The results of each model are presented in Table 4.

As it is observed in the last column of Table 4, the *p*-value of *F*-statistic in each model is lower than 0.05, which means that all models have good adaptation to the theoretical model. This is powerful evidence that our research is steady and our results are valid.

In the last step of analysis is the estimation of a logit model for every model (one for each lake). First authors estimate the fitting of each model by the logit fitting information test, the results of which are presented in Table 5.

As it is observed in the last column of the Table 5, the fit of the models is statistically significant while the *p*-value of all three tests is lower than 0.05, which means that the results of the logit estimation will be valid.

In Table 6, authors can see the results of the logit model (authors show only the statistically significant variables).

According to Table 6, authors can say for example for Kastoria, that if the citizens live next to the lake (X_{12}), the possibility to pay is higher, while the same possibility is also higher if the citizens have heritage next to the lake (X_{19}). On the other hand, the possibility to pay is lower if a good amount of money is offered to them in order to ignore the degradation of the lake (X_{14}). Similar results are excluded for every town.

4. Conclusions

According to the results of the empirical analysis, author can separate the conclusion in three different sections, each for every lake. About the lake of Kastoria (Orestiada), author found that the citizens are able to play higher amount of money for the restoration of the lake, while they believe that the protection of the lake is a crucial subject. The same WTP is increased if the citizen lives close to the lake, if the amount of money that would get as compensation is decreased, if he/she has heritage next to the lake and if his/her income is higher than the average of the local community.

About the lake of Ioannina (Pamvotida), author found that a citizen's WTP is increased if he/she visits the lake very often, if he/she believes that the appearance of the lake is awful, if he/she thinks that the local authorities are not able to take care of the problem and if he/she lives close to the lake.

Finally, about the lake of Florina (Cheimaditida), authors also found that a citizen's volition to pay for the preservation/restoration of the lake is increased, while the ecological condition of the lake is really bad. The same WTP is also increased if the citizen lives close to the lake and if the citizen is married.

According to the results above, authors cannot ignore the fact that those three important wetlands of Greece are degraded. Citizens who live next to those lakes declare to pay higher in order to restore the lake. This is evidence about the condition around these lakes. It is important to mention that there are different parameters that affect the citizens' WTP in every town. This is a normal fact because of the very different situation and living conditions in every town resulting in different requirements of local people. Last but not least, is the social dimension which appears in Florina, because if the citizen who declares "married", is willing to pay higher in order to restore the lake. It is probably a future concern because he/she wants his/her children to grow up in more healthy and beautiful environment. This study is about three big wetlands of Greece. It should be a part of a greater project about environmental protection which has to be supported by every single citizen and all authorities because the environmental pollution may lead to the human extinction.

References

[1] Barbier, E. B., Acreman, M. C., and Knowler, D. 1997. *Economic Valuation of Wetlands: A Guide for Policy Makers and Planners*. Ramsar Convention Bureau, Gland, Switzerland.

[2] Boyer, T., and Polasky, S. 2004. "Valuing Urban Wetlands: A Review of Non-market Valuation Studies." *Wetlands* 24 (4): 744-55.

[3] Brander, L., Florax, R., and Vermaat, J. 2006. "The Empirics of Wetland Valuation: A Comprehensive Summary and a Meta-Analysis of the Literature." *Environmental & Resource Economics* 33 (2): 223-50.

[4] Brouwer, R., Langford, I., Bateman, I., and Turner, R. 1999. "A Meta-Analysis of Wetland Contingent Valuation Studies." *Regional Environmental Change* 1 (1): 47-57.

[5] Fog, J., Lampio, T., Rooth, J., and Smart, M. 1982. *Managing Wetlands and Their Birds*. International waterfowl Research Bureau, Slimbridge, England.

[6] Kazmierczak, R. F. 2001. "Economic Linkages between Coastal Wetlands and Hunting and Fishing: A Review of Value Estimates Reported in the Published Literature." Louisiana State University Agricultural Center, Baton Rouge, Staff Paper 2001-2003.

[7] Kontogianni, A., Skourtos, M., Langford, I., Bateman, I., and Georgiou, S. 2001. "Integrating Stakeholder Analysis in Non-market Valuation of Environmental Assets." *Ecological Economics* 37 (1): 123-38.

[8] Mantzafleri, N., Psilovikos, A., and Blanta, A. 2009. "Water Quality Monitoring and Modeling in Lake Kastoria, Using GIS. Assessment and Management of Pollution Sources." *Water Resources Management* 23 (15): 3221-54.

Call for Papers

Dear author,

This is ***Journal of Environmental Science and Engineering*** A (ISSN 2162-5298) and ***Journal of Environmental Science and Engineering*** B (ISSN 2162-5263) (Earlier title: Journal of Environmental Science and Engineering, ISSN 1934-8932), a professional journal published across the United States by David Publishing Company, New York, NY 10034, USA.

Journal of Environmental Science and Engineering A (ISSN 2162-5298) and ***Journal of Environmental Science and Engineering*** B (ISSN 2162-5263) (Earlier title: Journal of Environmental Science and Engineering, ISSN 1934-8932) is collected and indexed by the Library of US Congress, on whose official website (http://catalog.loc.gov) an on-line inquiry can be triggered with its publication number ISSN 2162-5298 and ISSN 2162-5263 as key words in "Basic Search" column. In addition, these journals are also retrieved by some renowned databases:

- Google Scholar
- Chinese Database of CEPS, Airiti Inc. & OCLC
- Chinese Scientific Journals Database, VIP Corporation, Chongqing, P.R. China
- CSA Technology Research Database
- Ulrich's Periodicals Directory
- Summon Serials Solutions
- CAS (Chemical Abstracts Service)
- CiteFactor (USA)
- Proquest

David Publishing strives hard to provide the best platform for researchers and scholars worldwide to exchange their latest findings and results. Current columns involve Aquatic Environment, Atmospheric Environment, Environmental Monitoring, Environmental Risk and Assessment, Environmental Biology, Environmental Health and Toxicology, Municipal Solid Waste and Green Chemistry, Soil Environment, Energy and Environment, as well as Other Issues. All the published papers can be browsed on our website (www.davidpublisher.com).

Contribution Requirements:

1) Paper must be empirical or theoretical contributions without being published previously;
2) All other scholars' words or remarks as well as their origins must be indicated if quoted;
3) English title, abstract and key words should be prerequisite;
4) Patterns or forms should conform to the standard listed on our website.

Automatic paper submission system is strongly recommended, while E-mail attachment sent through email at environmentalAB@hotmail.com; environmental@davidpublishing.org is still available.

Please visit our website at www.davidpublisher.com for the automatic paper submission systems.
Should you have any questions or concerns feel free to contact us.

Best regards,
Journal of Environmental Science and Engineering
David Publishing Company

Journal of Environmental Science and Engineering A
Volume 7, Number 3, March 2018

David Publishing Company
616 Corporate Way, Suite 2-4876, Valley Cottage, NY 10989, USA
Tel: 1-323-984-7526, 323-410-1082; Fax: 1-323-984-7374, 323-908-0457
http://www.davidpublisher.com, www.davidpublisher.org
environmental@davidpublishing.org, environmental@davidpublishing.com